

The effect of water on the sulphur concentration at sulphide
saturation (SCSS) in natural melts

Marc-Antoine Fortin

Master of Science Degree

Earth & Planetary Sciences

McGill University

3450 rue University, H3A 0E8

Montréal

July 2014

Thesis submitted to McGill University in partial fulfillment of the requirements for the
degree of Master of Science

© Copyright Marc-Antoine Fortin, 2014

ABSTRACT

We experimentally investigated the effect of water on the sulphur concentration at sulphide saturation (SCSS) in basaltic, andesitic, and rhyolitic melt compositions at 1250 °C, 1 GPa, and oxygen fugacities buffered at or near the graphite-carbon dioxide (CCO) buffer in a piston-cylinder apparatus. We directly measured water concentrations in our sulphide saturated melts using Raman spectroscopy. Our experiments varied from anhydrous conditions up to 7.3 wt.% total dissolved water. Our results show an increase in the SCSS of about 100 ppm per wt.% added water in all melt compositions. We used data from our study and previous studies to create two models for calculating the SCSS as a function of temperature, pressure, melt composition, and total dissolved water. The first model, Model A, attempts to incorporate the effect of oxygen fugacity in the melt composition by discriminating between ferric and ferrous iron in its melt composition term, while the second model, Model B, uses mole fractions of major oxides as an approximation of the effect of melt composition on the SCSS. Despite Model B not including the effect of oxygen fugacity, we find that it calculates the SCSS of our calibrating dataset, as well as an independent test set, and a natural, high-Ni dataset to within about 5% relative variation, significantly better than Model A and within measurement uncertainties. We thus favour the empirical mole fractions of major oxides approach, with the following equation to determine the SCSS:

$$\ln(S, ppm) = 49.478 - \frac{5849.7}{T} - 325.37 \frac{P}{T} - 35.583 XH_2O - 40.365 XSiO_2 - 35.494 XTiO_2$$

$$- 39.202 XAl_2O_3 - 34.217 XFeO - 36.963 XMgO - 36.335 XCaO$$

$$- 35.641 XNa_2O - 46.392 XK_2O$$

where T is the temperature in Kelvin, P is the pressure in GPa, and X are the mole fractions of oxides. Our model shows an increase of the SCSS of about 100 ppm per wt.% added water for basaltic compositions, about 90 ppm for andesitic compositions, and about 45 ppm for rhyolitic melts. The model is applicable to Martian basaltic and terrestrial basaltic to rhyolitic melts at pressures from 1 atm to 5 GPa, temperatures from 1050 to 1800 °C, melt water concentrations from anhydrous to 7.3 wt.%, and oxygen fugacities under about 1.5 log unit below the nickel-nickel oxide oxygen buffer, NNO (where sulphide predominates).

RÉSUMÉ

Nous avons expérimentalement étudié l'effet de l'eau sur la concentration en soufre à saturation en sulfide (CSSS) dans des silicates fondus de compositions basaltique, andésitique, et rhyolitique à 1250 °C, 1 GPa, et une fugacité d'oxygène réglée ou approchée par le tampon graphite-dioxyde de carbone (CCO). Nous avons directement mesuré la concentration totale en eau de nos silicates fondus saturés en sulfides à l'aide de la spectroscopie Raman. La teneur en eau de nos expériences varie de complètement anhydre jusqu'à 7.3 % par poids d'eau totale dissoute. Nos résultats démontrent une augmentation de la valeur de la CSSS de l'ordre de 100 ppm lorsque la concentration totale en eau augmente d'un pourcent par poids, et ce dans toutes les compositions que nous avons étudiées. Nous avons combiné nos résultats avec ceux d'études antérieures afin de construire deux modèles qui peuvent calculer la CSSS en fonction de la température, la pression, la composition du silicate fondu, ainsi que la concentration totale d'eau dissoute. Le premier modèle, le Modèle A, tente d'incorporer l'effet de la fugacité d'oxygène sur la CSSS dans la composition du silicate fondu en discriminant entre les ions de fers ferreux et ferriques. Le deuxième modèle, Modèle B, utilise simplement la composition du silicate fondu en oxydes majeures, exprimé en fraction molaire. Bien que le Modèle B n'inclue pas directement l'effet qu'a la fugacité d'oxygène, nous notons qu'il calcule la CSSS de notre ensemble de données de calibration, ainsi que d'un ensemble de données testes et que d'un ensemble de

données naturelles qui contiennent une haute teneur en Ni à une variation de 5% près : ce qui est mieux que le Modèle A et que l'incertitude sur les mesures. Nous favorisons donc l'approximation de la composition de silicates fondus par leur concentration en oxydes majeurs pour calculer la CSSS, selon l'équation suivante :

$$\ln(S, ppm) = 49.478 - \frac{5849.7}{T} - 325.37 \frac{P}{T} - 35.583 XH_2O - 40.365 XSiO_2 - 35.494 XTiO_2 \\ - 39.202 XAl_2O_3 - 34.217 XFeO - 36.963 XMgO - 36.335 XCaO \\ - 35.641 XNa_2O - 46.392 XK_2O$$

où T est la température en Kelvin, P est la pression en GPa, et X sont les fractions molaires des oxydes stipulés. Notre modèle montre une augmentation de la CSSS de l'ordre de 100 ppm pour une augmentation de la concentration totale en eau d'un pourcent par poids pour les compositions basaltiques, d'environ 90 ppm pour les compositions andésitiques, et d'environ 45 ppm pour les silicates fondus de composition rhyolitique. Le model est applicable aux basaltes Martiens fondus ainsi qu'aux silicates fondus terrestres de compositions basaltiques à rhyolitiques à des pressions allant de 1 atm à 5 GPa, des températures de 1050 à 1800 °C, des teneurs en eau d'anhydre à 7.3 % par poids, et des fugacités d'oxygène inférieures à 1.5 unité logarithmique sous le tampon de fugacité d'oxygène de nickel-oxyde de nickel, NNO (où les sulfides prédominent).

ACKNOWLEDGEMENTS

18 experiments were analysed using the Raman spectrometer in Prof. Ian Butler's lab at McGill University by Jacqueline Riddle, and another 11 were analysed by Yan Lavergne. SIMS work on our basaltic standards was done by Eleanor Berryman as part of an unpublished undergraduate project at McGill University, working with Prof. Don R. Baker.

I would like to extend my greatest thanks to my advisor, Prof. Don R. Baker, for his thoughtful guidance and comments, and for his patience and availability throughout the course of this project. I would also like to thank Lang Shi for his support with the electron microprobe facilities at McGill University, Prof. Richard Hervig for his help with using the SIMS at Arizona State University, and Dr. Richard Bormett for his assistance with using the Raman spectrometer at Renishaw Canada Ltd.. Finally, I would like to thank Prof. Malcom J. Rutherford for his thoughtful comments which helped strengthen the arguments presented in this thesis.

TABLE OF CONTENTS

TABLE OF CONTENTS	7
LIST OF TABLES	8
LIST OF FIGURES.....	9
Chapter 1: Introduction.....	10
Background.....	12
Chapter 2: Experimental & Analytical Techniques.....	22
Experimental Methods	22
Melt composition analyses.....	26
Melt water concentration analyses	28
Chapter 3: Experimental Results	35
Chapter 4: Discussion	42
Effect of water on the SCSS	43
Factors controlling the SCSS	45
Chapter 5: Modelling the SCSS	48
Model A (MFM)	48
Model B (mole fractions of oxides):	50
Model calibration.....	52
Modelled effect of water on the SCSS.....	60
Chapter 6: Applications	63
Application to hydrous, experimental melts	63
Application to hydrous, Ni-rich natural melts	65
Chapter 7: Conclusions.....	69
REFERENCES.....	71
APPENDIX I	83
APPENDIX II	92
APPENDIX III	93

LIST OF TABLES

Table 1: Compositions of the starting silicate materials.....	23
Table 2: Calibration parameters for determination of water concentration from Raman spectroscopy.....	34
Table 3: Composition of our experimental melts saturated with a sulphide phase.....	38
Table 4: Fitting parameter coefficients for the characterisation of the SCSS	55

LIST OF FIGURES

Figure 1: The effect of water on the sulphur concentration at sulphide saturation (SCSS) as calculated using the model of Liu et al. (2007)	19
Figure 2: Two typical, Long (1977)-normalised Raman spectra of basaltic glasses with different water concentrations.	31
Figure 3: Backscattered electron microprobe image of a typical run product showing sulphide saturation.. ..	37
Figure 4: The sulphur concentration at sulphide saturation in the silicate melts of experiments as a function of the melt water concentration.	41
Figure 5: The modelled and measured SCSS for the calibration dataset	57
Figure 6: The relative difference between the calculated and the measured SCSS of the models.. ..	59
Figure 7: The effect of water on the SCSS, as calculated using Model B	61
Figure 8: The modelled and measured SCSS for the dataset of indirect hydrous studies	64
Figure 9: The modelled and measured SCSS for the hydrous, Ni-rich natural dataset of Ariskin et al. (2013).. ..	67

Chapter 1: Introduction

Sulphur is a volatile element present in all magmatic systems. It is one of the most abundant elements in Earth system fluids, alongside water and carbon dioxide. At oxygen fugacities greater than that of 1.5 log units above the nickel-nickel oxide buffer (NNO; Frost, 1991), the dominant sulphur species in silicate melts is sulphate (S^{6+}), and at oxygen fugacities below that, sulphide (S^{2-}) predominates (e.g., Fincham & Richardson, 1954; Carroll & Rutherford, 1985, 1987; Wallace & Carmichael, 1992; Wilke et al., 2008). The transition from predominately sulphide to sulphate in melts occurs over a range of oxygen fugacities of about the fayalite-magnetite-quartz oxygen buffer (FMQ; O'Neill, 1987), to about 2 log units above FMQ (Wallace & Carmichael, 1992). Because of the multiple species, and the uncertain nature of the transition zone, it is difficult to model and predict the behaviour of sulphur in systems where the oxygen fugacity is unknown (Baker & Moretti, 2011).

Sulphur plays an important role in many magmatic processes, but the behaviour of sulphur present in melts is still poorly understood (Behrens & Webster, 2011). A better

understanding of the storage and transport of sulphur would improve our modelling of the formation of a large variety of ore deposits (Simon & Ripley, 2011), and allow us to better monitor volcanoes (Oppenheimer et al., 2011), with the long-term goal of predicting their eruptions (Symonds et al., 1994). Sulphur is also important in the glass industry, where it is used during fining to increase the size of existing bubbles, and thus facilitates degassing (Muller-Simon, 2011). Although the effect of sulphur on these different systems varies, the factors controlling the behaviour of sulphur species remain the same: temperature, pressure, oxygen fugacity, melt composition, and water concentration.

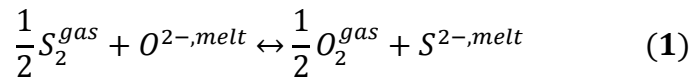
The sulphur concentration at sulphide saturation (SCSS) represents the maximum amount of sulphur a melt can dissolve at oxygen fugacities where S^{2-} predominates, and therefore provides an upper boundary to the sulphur concentrations found in melts at reduced oxygen fugacities. Previous studies investigated the saturation of silicate melts with a sulphide phase at various temperatures, pressures, and melt compositions, as well as oxygen and sulphur fugacities, but almost exclusively at anhydrous

conditions (e.g., Haughton et al., 1974; Shima & Naldrett, 1975; Danckwerth et al., 1979; Poulson & Ohmoto, 1990; Wallace & Carmichael, 1992; Mavrogenes & O'Neill, 1999; Holzheid & Grove, 2002; O'Neill & Mavrogenes, 2002; Li & Ripley, 2005; Jugo 2009). Despite the fact that most magmas contain measurable amounts of water (Sobolev & Chaussidon, 1996), only limited research has been conducted at hydrous conditions (e.g., Clemente et al., 2004; Scaillet & Pichavant, 2005; Liu et al., 2007; Moune et al., 2009; Li & Ripley, 2009; Ariskin et al., 2013; Ding et al., 2014). Our goal is to model how water—in addition to temperature, pressure, oxygen fugacity, and melt composition—affects the solubility of sulphide (e.g., FeS) in natural melts at sulphide saturation: the effect of water on the SCSS.

Background

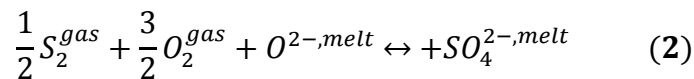
Researchers were first interested in the behaviour of sulphur in silicate melts for use as a way to control the amount of sulphur present in slags. Early experimentalists used simple synthetic oxide mixtures equilibrated with CO-CO₂-SO₂ or CO₂-H₂-SO₂ in gas-flow furnaces at 1 atm pressure. Using such a technique, Fincham & Richardson (1954)

described the mechanisms of sulphur dissolution in simple silicate melts coexisting with a gas phase at 1 atm. By compiling their and previous researchers' results, they found that at low oxygen fugacities, sulphur dissolves into the melt as sulphide, following the reaction:



where S_2^{gas} and O_2^{gas} are the S_2 and the O_2 in the gas phase, $S^{2-,melt}$ is the S^{2-} in the silicate melt phase, and $O^{2-,melt}$ is the free oxygen not associated with the silica tetrahedral network of the silicate melt.

At higher oxygen fugacities, sulphur dissolves as sulphate, as described by:



where $SO_4^{2-,melt}$ is the SO_4^{2-} in the silicate melt phase.

These reactions were later shown to be applicable to natural melts by Katsura & Nagashima (1974). Note that both reactions involve a coupled redox exchange of sulphur and oxygen species. Richardson & Fincham (1954) emphasised this by suggesting that the oxygen species linked with metal atoms are the only important

oxygen species for the dissolution of sulphur, and thus that the solubility of sulphur must be inversely proportional to the amount of silica. Building on previous work by Rosenqvist (1951), Fincham & Richardson (1954) defined the sulphide capacity (C_S) from equation (1) as:

$$C_S = [S] \frac{\sqrt{fO_2}}{\sqrt{fS_2}} \quad (3)$$

where $[S]$ is the concentration of sulphur in the melt expressed in weight percent, and fO_2 and fS_2 are the oxygen and sulphur fugacities. While its name might *a priori* seem to indicate otherwise, the C_S is not the maximum amount of sulphide that a melt can dissolve, or sulphide saturation. The C_S is a semi-equilibrium constant, as derived from equation 1. It is independent of the presence of a sulphide phase and depends only on the concentration of sulphur in the melt, and the oxygen and sulphur fugacities of the system (see equation 3).

Shima & Naldrett (1974) experimented with ultramafic melts at 1450 °C, 1 atm, and reduced oxygen fugacities, and in some instances saturated with an iron sulphide phase. They were the first to introduce the concept of the SCSS: the amount of sulphur

present in a melt coexisting at equilibrium with a sulphide phase. Haughton et al. (1974) investigated the SCSS in experiments on natural melts equilibrated with CO-CO₂-SO₂ gas mixtures at 1200 °C, 1 bar, and oxygen fugacities where sulphide was the dominant sulphur species in the melt. Their innovative use of electron microprobe techniques—unlike previous studies, which used bulk wet chemistry—allowed them to analyse melts separately from their coexisting sulphide phases. Haughton et al. (1974) were able to show a positive correlation between the oxygen fugacity and the SCSS at constant sulphur fugacity. Additionally, they found a positive relationship between the SCSS and the sulphur fugacity at constant oxygen fugacity. Because of the compositional variations of the melts they studied, Haughton et al. (1974) were able to construct a model to calculate the C_s that was applicable to natural basaltic compositions. Their model is dominated by the influence of the concentration of FeO in the melt, and less influenced by the CaO, MgO, TiO₂, NaO and K₂O concentrations. Because of the nature of the C_s , the model of Haughton et al. (1974) requires estimates of both oxygen and sulphur fugacities in order to calculate the SCSS. The findings of Haughton et al. (1974)

were later supported by Wendlandt (1982), who investigated the effect of pressure and melt composition on the SCSS.

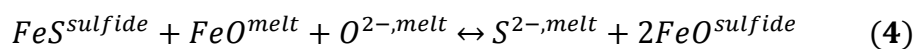
Wallace & Carmichael (1992) reviewed and compiled measurements from previous studies to build a model to calculate the mole fraction of sulphur in basaltic melts at 1 atm at specified oxygen and sulphur fugacities. Similarly to Haughton et al. (1974), and as emphasised by Poulson & Ohmoto (1990), Wallace & Carmichael (1992)'s model is highly dependent on the FeO concentration of the melt. The model also incorporates as parameters the mole fractions of SiO₂, CaO, and (Na₂O + K₂O). Although the model of Wallace & Carmichael (1992) accurately predicted sulphur concentrations for melts of compositions similar to that of their database, it overestimated the sulphur concentrations of more silicic melt compositions. This emphasises the need for a varied dataset when constructing empirical models for application to natural systems that exhibit a wide range in conditions.

O'Neill & Mavrogenes (2002) used their own experimental results and the Gibbs free energy for reactions involving iron, sulphur, and oxygen between gas, silicate and

sulphide phases to create a model of the C_S at 1 bar. The work of O'Neill & Mavrogenes (2002) revalidated the effect of composition on the solubility of sulphur. Holzheid & Grove (2002) added a non-bridging oxygen-to-tetrahedral cation ratio term (NBO/T, Mysen & Richet, 2005) to the high-pressure SCSS model of Mavrogenes & O'Neill (1999) in order to more accurately account for the influence of melt composition.

Liu et al. (2007) experimentally investigated the effect of temperature, pressure, melt composition, oxygen fugacity, and water on the SCSS in basaltic to rhyolitic melts ranging from temperatures of 1050 to 1450 °C at 500 MPa and 1 GPa. They created a model of the SCSS based on a reaction describing the dissolution of sulphide, following

Wendlandt (1982):



where $FeS^{sulfide}$ and $FeO^{sulfide}$ represent the FeS and FeO in the sulfide phase, and FeO^{melt} represents the FeO in the silicate melt phase. They set the activity of $FeO^{sulfide}$ as a constant and the activity of $FeS^{sulfide}$ to unity, based on the small concentration of $FeO^{sulfide}$, and used concentrations of FeO^{melt} and $S^{2-,melt}$ as proxies for their respective

activities. Liu et al. (2007) defined a new parameter as an estimate for the activity of O^{2-} in melt. This new parameter, the MFM—a modified FM parameter (Ryerson & Watson, 1987)—accounts for the effects of melt composition on the SCSS:

$$MFM = \frac{Na + K + 2(Ca + Mg + Fe^{2+})}{Si (Al + Fe^{3+})} \quad (5)$$

where the element symbol is the mole fraction of that element in the melt. Similarly to previous studies, the model predicts an increase of the SCSS for an increase in temperature or for decreases in pressure or the silica concentration of the melt. The model also predicts an increase of the SCSS with addition of water to silicic melts, but a decrease of the SCSS with the addition of water to mafic magmas. The effect of water in Liu et al. (2007)'s model is even more irregular at low water concentrations, as shown in Figure 1 for a MORB composition at 1350°C, 1 GPa, and an oxygen fugacity at or near the graphite-carbon monoxide oxygen buffer (CCO; Jakobsson & Oskarsson, 1994).

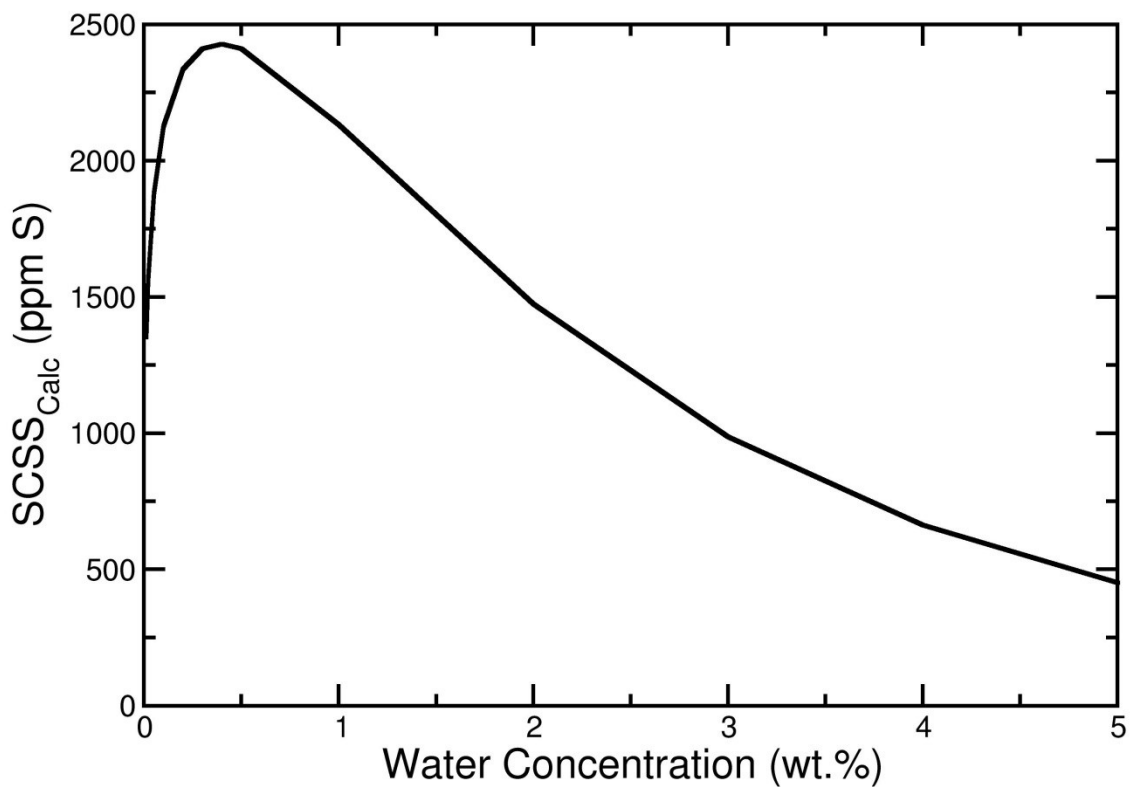


Figure 1: The effect of water on the sulphur concentration at sulphide saturation (SCSS) as calculated using the model of Liu et al. (2007) on a melt of MORB composition at 1350°C, 1 GPa, and at or near CCO. The model shows an increase followed by a decrease in the SCSS as the total water concentration in the melt is increased.

Moune et al. (2009) investigated the saturation of hydrous basaltic and basaltic-andesitic melts with pyrrhotite or molten FeS. For melts with low water concentrations, Moune et al. (2009)'s values were accurately predicted by the model of Liu et al. (2007), but at water-saturated conditions, measured SCSS values were up to an order of magnitude greater than calculated. Moune et al. (2009)'s experimental results suggest a positive relationship between increasing water concentrations and the SCSS. The positive effect of water on the sulphur concentration is also in disagreement with the thermodynamic model of Moretti et al. (2003), which states that the concentration of sulphide in the melt decreases with increasing total melt water concentration.

Li & Ripley (2009) updated the anhydrous SCSS model of Li & Ripley (2005) by fitting a dataset of hydrous experimental results compiled from previous studies. Their model describes the mole fraction of sulphur in a silicate melt at sulphide saturation as a function of mole fractions of oxides, water concentration of the melt, temperature, and pressure. Most recently, Ariskin et al. (2013) generated a model of the solubility of sulphur in mafic and ultramafic silicate melts that accounts for the effects of

temperature, pressure, oxygen fugacity, and melt composition and Ni concentration.

The Ariskin et al. (2013) model is based on the hypothesis that positively-charged Fe-Ni sulphide complexes (e.g., $(\text{Fe}_y\text{Ni}_{1-y})_z\text{S}^{2(z-1)+}$) exist in the melt, although they present no supporting evidence for such complexes. Their calibration dataset includes mostly anhydrous experimental glass analyses, and measurements of natural samples they believe to be at sulphide saturation. Interestingly, and similarly to Moune et al. (2009), Ariskin et al. (2013) find a positive correlation between the SCSS and the water concentration of the melt.

The conflicting conclusions from the above models demonstrate our poor understanding of the effect of water on the SCSS and demands further investigation. Further, the availability and diversity of hydrous measurements of the SCSS are limited, thus our goal of experimentally investigating and modelling the effect of water on the SCSS.

Chapter 2: Experimental & Analytical Techniques

Experimental Methods

We conducted experiments using a piston-cylinder apparatus with rock powders enriched with sulphur (as FeS) to synthesise sulphide saturated melts. We chose to experiment with a variety of melt compositions to account for the effect of melt composition on the SCSS (e.g., Wallace & Carmichael, 1992; O'Neill & Mavrogenes, 2002). Following Liu et al. (2007), we chose to use two basalts (Etna basalt and MORB), an andesite (AG7-1) from Agrigan in the Northern Mariana Arc (Stern, 1979), and a rhyolite (LCO), the Lake County obsidian (Harrison & Watson, 1983). We report the compositions of the starting materials, as analysed by Liu et al. (2007) by electron microprobe, in Table 1. We doped each starting material with about 5000 ppm sulphur, added as pyrrhotite (Fe_{1-x}S), in order to saturate the resulting melt in a sulphide phase. The Etna basalt enriched with about 5000 ppm S was prepared by Liu et al. (2007) using cleaned, crushed pyrrhotite and mixed into the rock powder using a mortar and pestle under alcohol for 1 hour to ensure homogeneity. The MORB sample, enriched

Table 1: Compositions of the starting silicate materials

Compositions of the starting silicate materials

Oxide (wt.%)	MORB basalt	Etna basalt	AG7-1 andesite	LCO rhyolite
SiO ₂	47.13	51.0	60.1	75.85
TiO ₂	1.72	1.28	0.81	0.11
Al ₂ O ₃	16.6	15.8	16.0	13.0
FeO*	10.9	7.95	8.80	0.79
MnO	0.18	0.18	0.22	0.09
MgO	6.3	9.16	1.87	0.07
CaO	10.61	11.4	5.81	0.57
Na ₂ O	3.15	2.52	4.25	4.19
K ₂ O	1.82	<d.l.	2.06	4.74
P ₂ O ₅	0.53	0.11	0.35	<d.l.
Total	98.94	99.4	100.27	99.41

<d.l. Below the detection limit of the electron probe.

Data from Table 1 of Liu et al. (2007).

with about 5000 ppm S rock powder used for experiments MAF-1, -4, -7, -9, and -12, was also prepared by Liu et al. (2007) using the same method. We prepared all other starting materials using the same technique employed by Liu et al. (2007).

To ensure that our experiments took place within the realm of sulphide predominance in the melt, rather than sulphate (Wilke et al., 2011), we packed between 0.010g and 0.015g of pyrrhotite-enriched rock powder into 3 mm long graphite capsules. These capsules buffer the oxygen fugacity in our systems to, or near that of the graphite-carbon monoxide oxygen buffer (CCO; Jakobsson & Oskarsson, 1994). At our experimental conditions of 1250 °C and 1 GPa, CCO is about 1.5-2 log units below the FMQ oxygen buffer (O'Neill, 1987), or at an absolute $\log(fO_2)$ of -8.87 (Jakobsson & Oskarsson, 1994) at these conditions, with no added water. At high water concentrations in the system, the oxygen fugacity of the system cannot be approximated by the CCO buffer anymore, and the exact oxygen fugacity is unknown. However, from sulphur peak shift analyses (Carroll & Rutherford, 1985), we find that all of our experiments occurred within the realm of sulphide predominance as the

composition of the sulphur phase was over 97% sulphide in even our most hydrous experiments.

We added to our starting compositions between 0.9 to 9.8 wt.% of distilled water using a 10 μ L syringe, before closing it with a matching graphite lid. We then placed the filled graphite capsule in a 9 mm long, 3 mm inner-diameter platinum capsule that we then crimped and welded shut. In addition to buffering the oxygen fugacity of the system to values where the predominant sulphur species is sulphide, this double capsule setup (i.e., graphite in platinum) also helps minimise the loss of both iron and sulphur from the melt to the outer Pt-capsule. The sealed platinum capsules were left to dry for a minimum of two hours in a 110 °C oven, then weighed again to insure that they were welded properly, and that no water was lost. For anhydrous samples, we placed the still-open platinum capsules in a 110 °C oven for a minimum of two hours before welding them, to ensure that the starting compositions were close to anhydrous. We performed all welding using a Lambert arc welder under Ar-gas.

The piston-cylinder apparatus allows us to mimic magmatic conditions in the deep crust of 1250 °C and 1 GPa, or about 33 km depth. Following Baker (2004), we used 1.91 cm diameter crushable alumina-Pyrex-NaCl assemblies to perform our experiments in a piston-cylinder apparatus at McGill University. We used C-type thermocouples to measure the temperature of our runs and automatically controlled it to 1250 ± 2 °C. After 6 hours, we quenched the experiment by turning off the power and allowing the run temperature to rapidly decrease to room temperature at an initial rate of 2000 °C/min, while maintaining constant pressure. This produced a quenched melt with a composition representative of the equilibrium melt at 1250 °C and 1 GPa.

Melt composition analyses

To analyse our samples, we first mounted them in 1 inch diameter epoxy disks and polished them by hand using polishing paper of decreasing grit, finishing with 1 µm, and then 0.3 µm particle-size alumina powder. Because rhyolitic glasses (LCO) are clear, we polished them in their platinum and graphite capsules to expose the quenched melts for this composition. For all other compositions we pried open the capsules and

separated the quenched melt using tweezers. We used electron microprobe analyses (EMPA) to determine the sulphur and major element concentrations in our quenched silicate melts saturated with sulphide. We analysed all of our run products using wavelength-dispersive spectrometry (WDS) with the JEOL JXA-8900L electron microprobe and its ZAF correction routine at the Electron Microprobe Microanalytical Facility at McGill University. We performed all of our analyses at an accelerating voltage of 15 kV, with a beam current of 20 nA, and a beam diameter of 10 μm . We used a counting time of 20 s for the peaks of major elements, and a background counting time of 10 s. For our analyses of S in the quenched melts, we used a peak counting time of 120 s for basalts, and 200 s for andesites and rhyolites. The background counting time was 60 s for basalts and 100 s for the more silicic compositions. This allowed us to lower the detection limit of S in our silicic samples to about 100 ppm. For our calibration, we used a synthetic pyrrhotite standard for S; a basaltic glass, VG-A99 (Jarosewich et al., 1979), for Na, Al, Fe, Si, Mg, Ca, and Ti; a rhyolitic glass for K; a spessartine for Mn; and a fluorapatite for P. We used a basaltic glass, VG-2 (Jarosewich et al., 1979), as a

secondary standard to check our calibrations. We measured the S concentration in this standard at 1402 ± 28 ppm, based upon 4 analyses done throughout the course of this study. This is in agreement with previous measurements of the sulphur concentration in this same glass: 1414 ± 30 ppm (Liu et al., 2007), 1403 ± 30 ppm (O'Neill and Mavrogenes, 2002), 1416 ± 36 ppm (De Hoog et al., 2001), 1420 ± 20 ppm by EMPA, and 1320 ± 50 ppm by wet chemistry (Wallace & Carmichael, 1992).

Melt water concentration analyses

The presence of water in some of our graphite-lined capsules can potentially alter the oxygen fugacity in our experiments, thus also impacting the water concentration of the melt. This behavior has not been observed in previous measurements of quenched melts in graphite capsules (e.g., Baker, 1991). To minimise this effect, we have opted to directly determine the concentration of water dissolved in our quenched melts by using Raman spectroscopy.

Several microanalytical techniques capable of high spatial resolution and high accuracy have been applied by previous researchers to characterise dissolved water in glasses,

such as infrared spectroscopy (e.g., Stolper, 1982; Beermann et al., 2011), electron microprobe “by-difference” (e.g., Devine et al., 1995; Clemente et al., 2004; Beermann et al., 2011; Jago & Dasgupta, 2013), or secondary ion mass-spectroscopy (SIMS; e.g., King et al., 2002). A disadvantage of using IR measurements to determine the water concentration of a glass is that the analysis must be done on a doubly-polished, micron-thick wafer. Electron microprobe techniques do not allow for direct measurements of light elements such as H, and thus this method only provides an indirect estimation from the difference from 100 wt.% of the sum of the measured oxides (Devine et al., 1995). Applying SIMS techniques to large sample sets is difficult because of limited access to these instruments. Raman spectroscopy offers a high spatial resolution (1-2 μm), readily available technique for the characterisation of total water dissolved in glasses (e.g., Thomas, 2000; Chabiron et al., 2004; Behrens et al., 2006; Le Losq et al., 2012).

Raman spectroscopy allows us to quantify the absorption of the glass due to molecular vibrations. We applied the technique at wavelengths varying from 100 to 1500 cm^{-1} , and 2600 to 4000 cm^{-1} . After obtaining our measurements, we corrected for elastic

scattering following Long (1977) and normalised to the highest intensity over the frequency range. The 3550 cm⁻¹ band is associated with the OH stretching vibration band, and the various peaks present in the region 100 to 1500 cm⁻¹ are linked to silicate absorption bands. Following the methods of Behrens et al. (2006), we use the ratio of the two regions' integrated intensity to accurately determine water concentrations in our quenched melt samples by using a simple linear relationship:

$$H_2O = m \frac{A_{3550}^*}{A_{LW-LC}^*} + b \quad (6)$$

where H₂O is the total water concentration of the melt in weight percent (wt.%), A^{*3550} is the area under the 3550 cm⁻¹ band, A^{*LW-LC} is the area under the 100-1500 cm⁻¹ region, and m and b are linear fitting parameters. Figure 2 displays two typical spectra obtained by Raman spectroscopy from a basaltic glass sample: one with 3.3±0.5 wt.% dissolved water, and the other with <0.4 wt.% water (the minimum quantifiable based upon our standards, as determined by the intercept 'b'). As expected, the spectrum of a higher water-concentration glass has a larger and broader water band around 3550 cm⁻¹ than the low water-concentration glass.

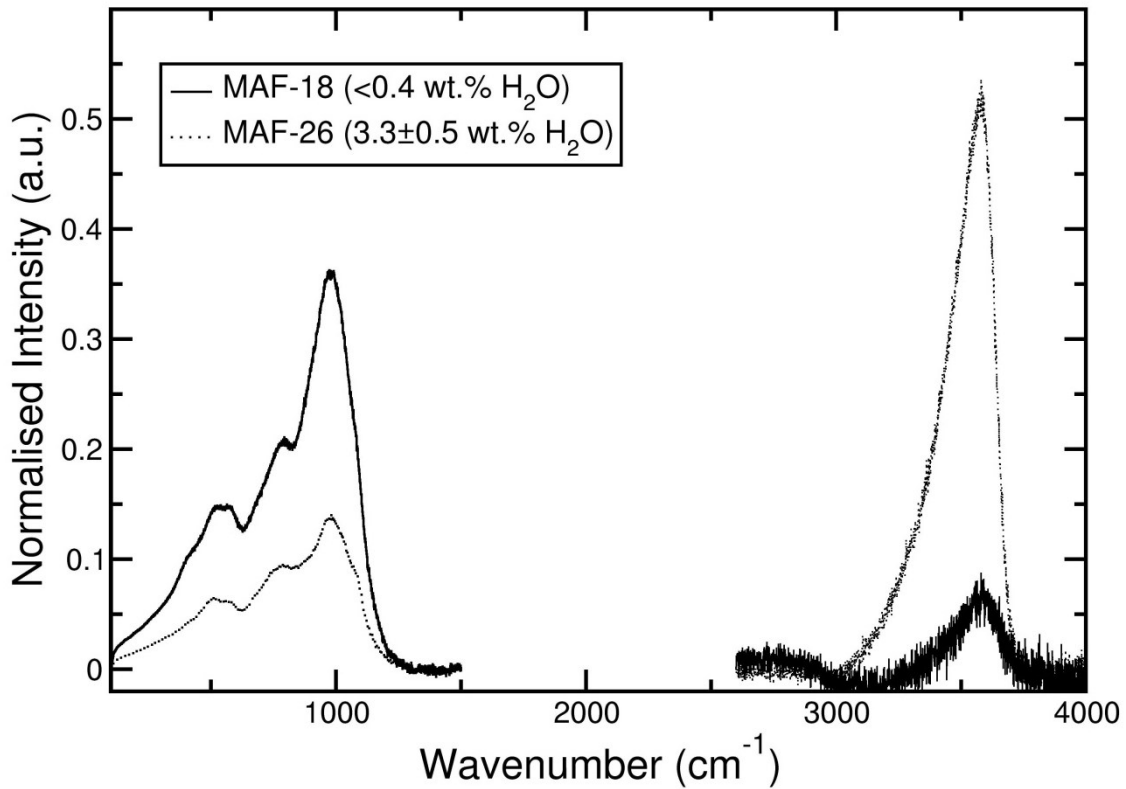


Figure 2: Two typical, Long (1977)-normalised Raman spectra of basaltic glasses with different water concentrations after their backgrounds have been removed. The spectrum represented by the dotted line is associated with a glass with <0.4 wt.% dissolved total water (MAF18), while the spectrum shown by a solid line is associated with a glass containing 3.3 ± 0.5 wt.% total dissolved water (MAF-26). The spectrum associated with the higher total water concentration shows a broader, larger peak centred at around a wavenumber of 3550 cm^{-1} .

To accurately determine the dissolved water concentration of our run products, we must compare the spectra we obtain to those of samples with a known water concentration. Thus, we generated a set of standard glasses with various amounts of water using the same starting compositions and analysed them with SIMS. We synthesised all standards at McGill University using a piston-cylinder apparatus and following the same capsule design that we used for our other experiments, at 1 GPa and 1250 °C. We analysed the water concentration of our standards by SIMS at the Secondary Ion Mass Spectrometry Labs at Arizona State University in Tempe, AZ with a CAMECA IMS 6F SIMS using standards M3N, M6N, PCDA, (Devine et al., 1995), and LPR and 2N internal standards, for rhyolitic compositions, and using standards SAT-M12-2 and Mas-12 (Moore et al., 1998) for andesitic compositions. After pre-sputtering the analysis points for 400 s, we used a focused O²⁻ beam at 8 keV and 13 nA to determine the water concentrations of our unknowns by comparing their ¹H/³⁰Si ratios to the standards'.

We were then able to construct calibration lines for analysing total water concentration by Raman spectroscopy in our basaltic, andesitic, and rhyolitic sets of samples. Table 2 shows the parameters we used in constructing our calibration lines following equation 6. We find a slope of 1.9968 a.u./cm⁻¹ for basaltic compositions, 1.3697 a.u./cm⁻¹ for andesitic compositions, and 0.4293 a.u./cm⁻¹ for rhyolitic compositions.

Behrens et al. (2006) combined both andesitic and basaltic compositions into the same equation. They found a higher slope than we do for our individual basalt or andesite calibration lines (3.66 a.u./cm⁻¹). Similarly, their unique calibration for albitic, haplogranitic, and dacitic compositions has a much higher slope than our calibration for our rhyolitic composition (5.135 a.u./cm⁻¹). Le Losq et al. (2012) emphasise the need for individual instruments and compositions to have their own calibrations, and we are therefore confident that our calibration lines are accurate for our measurements.

Table 2: Calibration parameters for determination of water concentration from Raman spectroscopy. $H_2O = m \times x + b$

Composition	n*	H ₂ O range†	m	SE‡	b	SE‡	R ² **
MORB (basalt)	3	0.31-6.46	1.9968	0.0310	-0.3713	0.0638	0.9998
AG7-1 (andesite)	5	0.06-6.58	1.3697	0.3411	-0.3640	1.0227	0.8431
LCO (rhyolite)	4	0.08-5.64	0.4293	0.4615	-0.4559	0.0520	0.9715

*Number of standards used for construction of the calibration line.

†Range of water concentration of the standards, in weight percent, as determined by SIMS.

‡Standard error.

**Coefficient of determination (R-squared).

Chapter 3: Experimental Results

We conducted all of our experiments at 1250 °C, 1 GPa for 6 hours. Because of the presence of graphite in our systems, we assume that the oxygen fugacity in our experiments was set at or near the CCO-buffer (i.e., $\log(fO_2)=-8.87$; Jakobsson & Oskarsson, 1994). In most cases, the run products of our experiments were a silicate melt phase coexisting with an immiscible sulphide melt phase, however, in run number MAF-12, a pyroxene phase was also present. We believe these crystals were formed during quenching, and are not the result of equilibrium crystallisation, because no other experiments (all run at the same conditions) showed crystallinity. Further, we did not observe vesicles or bubbles in any of our experiments. This suggests that our capsules were not saturated with a volatile phase. We confirmed that our experiments took place within the realm of sulphide predominance through peak shift tests from EMPA, where we found all of the sulphide blebs to be dominated by sulphide species (Carroll & Rutherford, 1985). The sulphide phase was present in all of our experiments as bright

yellow spheres ranging from less than 1 to almost 100 μm in diameter, as shown in Figure 3.

The presence of a distinct sulphide phase confirms that our experiments reached sulphide saturation. We report our analyses of the silicate melt phases in Table 3, along their standard deviations (1σ). We analysed major element compositions, as well as sulphur concentrations by electron microprobe, and water concentrations with Raman spectroscopy.

Six hours appear sufficient for the studied systems to reach equilibrium based on the previous study of Liu et al. (2007). Liu et al. (2007) demonstrated that their experiments were able to reach equilibrium after 6 hours, using the same starting materials, experimental apparatus, methods, and under the same conditions as this study. Additionally, we ran a dry experiment for 24 hours (MAF-29) to test for equilibrium. Because the sulphur concentration of the melt phase of run MAF-29 (1018 ± 23 ppm) is within one standard deviation of another dry experiment of the same composition that

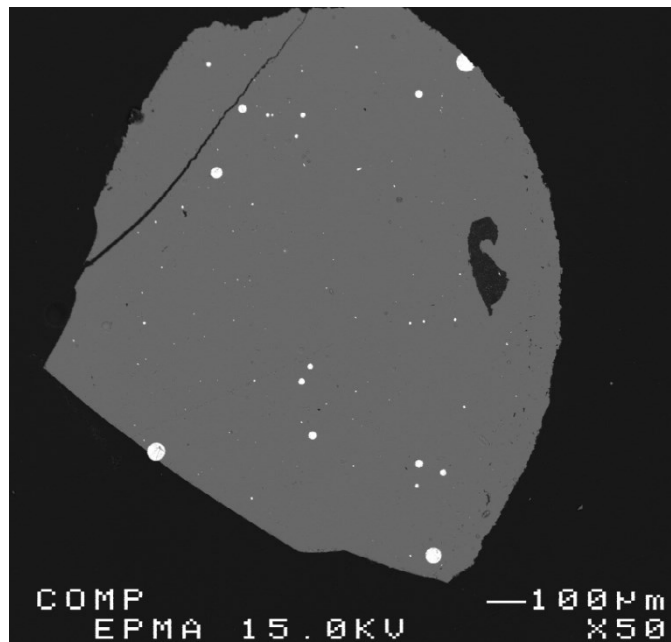


Figure 3: Backscattered electron microprobe image of MAF-27, a typical run product, showing sulphide saturation. The light grey phase is the quenched glass, and the white, rounded spots are of an immiscible sulphide quenched melt.

Table 3: Composition of our experimental melts saturated with a sulphide phase

Sample	‡SiO ₂	TiO ₂	Al ₂ O ₃	FeO	MnO	MgO	CaO	Na ₂ O	K ₂ O	P ₂ O ₅	S (ppm)	Total	H ₂ O ⁺	H ₂ O†
<i>Etna basalt + 5000 ppm S</i>														
MAF-1	47.7 (3)	1.66 (4)	16.6 (2)	10.2 (2)	0.18 (3)	6.2 (1)	10.8 (1)	3.26 (7)	1.87 (4)	0.53 (2)	874 (48)	99.3	2.2	3.1 (5)
MAF-2	47.8 (2)	1.66 (7)	16.7 (2)	10.2 (2)	0.18 (3)	6.2 (1)	10.7 (1)	3.19 (4)	1.84 (3)	0.52 (3)	870 (56)	99.3	0.0	0.5 (1)
MAF-8	46.5 (2)	1.66 (5)	15.9 (2)	9.7 (2)	0.16 (4)	6.0 (1)	10.6 (1)	3.08 (6)	1.78 (6)	0.51 (3)	943 (34)	96.3	1.5	4.7 (7)
MAF-14	47.0 (2)	1.85 (6)	16.2 (1)	9.4 (2)	0.17 (3)	6.2 (1)	10.9 (1)	3.10 (6)	1.65 (5)	0.55 (2)	865 (47)	97.4	4.0	1.6 (2)
MAF-18	47.6 (2)	1.78 (7)	16.6 (2)	10.3 (2)	0.17 (3)	6.0 (1)	10.7 (1)	3.25 (7)	1.81 (7)	0.52 (4)	929 (127)	99.1	0.0	0.0 (4)
MAF-20	47.4 (2)	1.7 (5)	16.4 (1)	7.99 (2)	0.17 (4)	6.2 (1)	11.0 (1)	3.17 (7)	1.77 (4)	0.53 (3)	1084 (47)	96.7	1.9	5.5 (8)
MAF-22	48.1 (2)	1.80 (7)	16.7 (1)	8.65 (1)	0.16 (4)	6.0 (1)	10.7 (1)	3.18 (5)	1.76 (4)	0.52 (3)	1068 (42)	97.9	3.1	1.9 (3)
MAF-26	46.5 (2)	1.75 (6)	16. (1)	9.04 (2)	0.15 (3)	6.0 (1)	10.5 (1)	3.08 (5)	1.69 (4)	0.53 (4)	1004 (32)	95.6	3.8	3.3 (5)
MAF-29*	47.4 (3)	1.67 (4)	16.8 (1)	9.93 (2)	0.15 (3)	6.3 (1)	10.8 (2)	3.38 (4)	1.84 (4)	0.56 (3)	1018 (23)	99.2	0.0	n/a
<i>MORB + 5000 ppm S</i>														
MAF-4	49.9 (2)	1.38 (5)	16.6 (1)	10.5 (2)	0.16 (5)	7.8 (1)	10.8 (1)	2.71 (6)	0.12 (1)	0.12 (1)	1180 (35)	100.4	0.0	0.9 (1)
MAF-7	49.8 (2)	1.31 (5)	15.8 (2)	10.1 (2)	0.17 (4)	8.6 (1)	11.2 (1)	2.48 (7)	0.09 (1)	0.11 (1)	1246 (34)	100	2.7	0.7 (1)
MAF-9	50.2 (2)	1.26 (6)	15.4 (2)	9.0 (3)	0.17 (4)	9.1 (1)	11.5 (1)	2.39 (3)	0.10 (2)	0.10 (1)	1248 (54)	99.5	0.9	2.6 (4)
MAF-12	49.6 (4)	1.33 (6)	14.9 (1)	8.1 (3)	0.15 (5)	8.6 (5)	11.3 (5)	2.2 (2)	0.09 (2)	0.09 (2)	1765 (33)	96.8	3.5	5.9 (9)
MAF-15	48.9 (3)	1.31 (5)	14. (1)	9.6 (2)	0.15 (3)	8.8 (1)	11.3 (1)	2.32 (5)	0.09 (1)	0.10 (2)	1409 (39)	97.6	4.1	2.8 (4)
MAF-19	49.7 (2)	1.41 (6)	16.1 (3)	10.3 (2)	0.17 (3)	7.8 (2)	10.8 (1)	2.65 (4)	0.10 (1)	0.11 (2)	1218 (40)	99.6	0.0	0.0 (4)

Sample	‡SiO ₂	TiO ₂	Al ₂ O ₃	FeO	MnO	MgO	CaO	Na ₂ O	K ₂ O	P ₂ O ₅	S (ppm)	Total	H ₂ O*	H ₂ O†
<i>AG7-1 andesite + 5000 ppm S</i>														
MAF-28	59.1 (6)	0.80 (5)	15.9 (1)	8.5 (1)	0.25 (4)	1.97 (4)	5.67 (6)	4.06 (4)	1.97 (3)	0.39 (4)	707 (45)	98.9	0.0	0.0 (4)
MAF-32	58.9 (4)	0.80 (4)	15.6 (1)	7.9 (2)	0.23 (5)	1.92 (4)	5.54 (7)	3.97 (8)	1.97 (4)	0.38 (3)	776 (29)	97.5	1.0	4.4 (7)
MAF-34	59.0 (2)	0.79 (4)	15.6 (1)	7.8 (2)	0.23 (4)	1.93 (6)	5.54 (7)	3.91 (5)	1.94 (5)	0.38 (3)	615 (35)	97.4	2.2	2.1 (3)
MAF-36	58.5 (2)	0.78 (3)	15.4 (1)	7.7 (2)	0.23 (4)	1.90 (2)	5.41 (5)	3.74 (4)	1.92 (4)	0.38 (3)	1094 (26)	96.2	3.3	4.1 (6)
MAF-38	58.3 (3)	0.82 (6)	15.4 (1)	7.7 (1)	0.20 (2)	1.88 (5)	5.4 (1)	3.65 (6)	1.87 (3)	0.37 (2)	1167 (22)	95.9	4.6	4.6 (7)
MAF-45	58.0 (3)	0.79 (3)	15.3 (1)	7.7 (2)	0.22 (6)	1.88 (8)	5.4 (1)	3.52 (6)	1.73 (4)	0.36 (2)	1265 (43)	95.3	6.1	7.3 (1)
<i>LCO rhyolite + 5000 ppm S</i>														
MAF-27	75.7 (3)	0.12 (3)	12.9 (1)	0.67 (6)	<d.l.	<d.l.	0.56 (4)	4.0 (1)	4.72 (5)	<d.l.	181 (29)	98.9	0.0	0.0 (5)
MAF-31	75.3 (3)	0.11 (4)	12.9 (1)	0.67 (7)	<d.l.	<d.l.	0.54 (2)	3.85 (4)	4.61 (6)	<d.l.	222 (42)	98.2	1.3	0.0 (5)
MAF-33	75.0 (3)	0.11 (3)	12.8 (1)	0.85 (9)	<d.l.	<d.l.	0.55 (4)	3.83 (8)	4.58 (5)	<d.l.	181 (33)	98	2.4	0.0 (5)
MAF-35	75.7 (2)	0.12 (4)	13.0 (1)	0.59 (7)	<d.l.	<d.l.	0.55 (3)	3.99 (4)	4.75 (7)	<d.l.	143 (20)	99	3.4	0.0 (5)
MAF-39	73.9 (2)	0.10 (4)	12.6 (1)	0.81 (6)	<d.l.	<d.l.	0.54 (2)	3.57 (6)	4.35 (7)	<d.l.	480 (22)	96.2	4.3	3.4 (5)
MAF-44	72.6 (4)	0.10 (4)	12.3 (1)	0.97 (8)	<d.l.	<d.l.	0.55 (3)	3.37 (7)	4.02 (6)	<d.l.	595 (29)	94.3	6.1	4.2 (6)

All experiments were ran at 1523.15 K, 1 GPa, and log (fO₂)=-8.87 for 6 hours

*Experiment MAF-29 was ran for 33 hours

‡Oxide analyses, in weight percent, by electron microprobe

*Added water concentration in weight percent, as weighted before experimental run

†Water concentration in weight percent, as determined by Raman spectroscopy

Numbers in parentheses are the last significant figures of standard deviation (1σ) based on the mean of the multiple analyses of the melt

<d.l., below the detection limit of the electron microprobe

n/a, not analysed

was ran for only 6 hours (MAF-18; 929 ± 127 ppm), we conclude that our experiments closely approached or reached equilibrium. Additionally, because we expect hydrous experiments to reach equilibrium more rapidly than anhydrous experiments, we infer that our hydrous experiments also reached equilibrium after an experimental run time of 6 hours.

We observe an increase of the SCSS with increasing water concentration in our experiments, as shown in Figure 4. We witness a relative increase of the SCSS in all studied melt compositions with increasing amounts of dissolved water. Of particular interest is the similarity in slopes of the different compositions. While basalts have about 50% higher sulphur solubilities than andesites, which themselves are about 30% higher than rhyolites', the three studied compositions show a positive, average slope of 93 ± 4 ppm S/wt.% H_2O or 1671 ppm S/mole fraction H_2O . This suggests that the mechanism behind the correlation is independent of the melt composition.

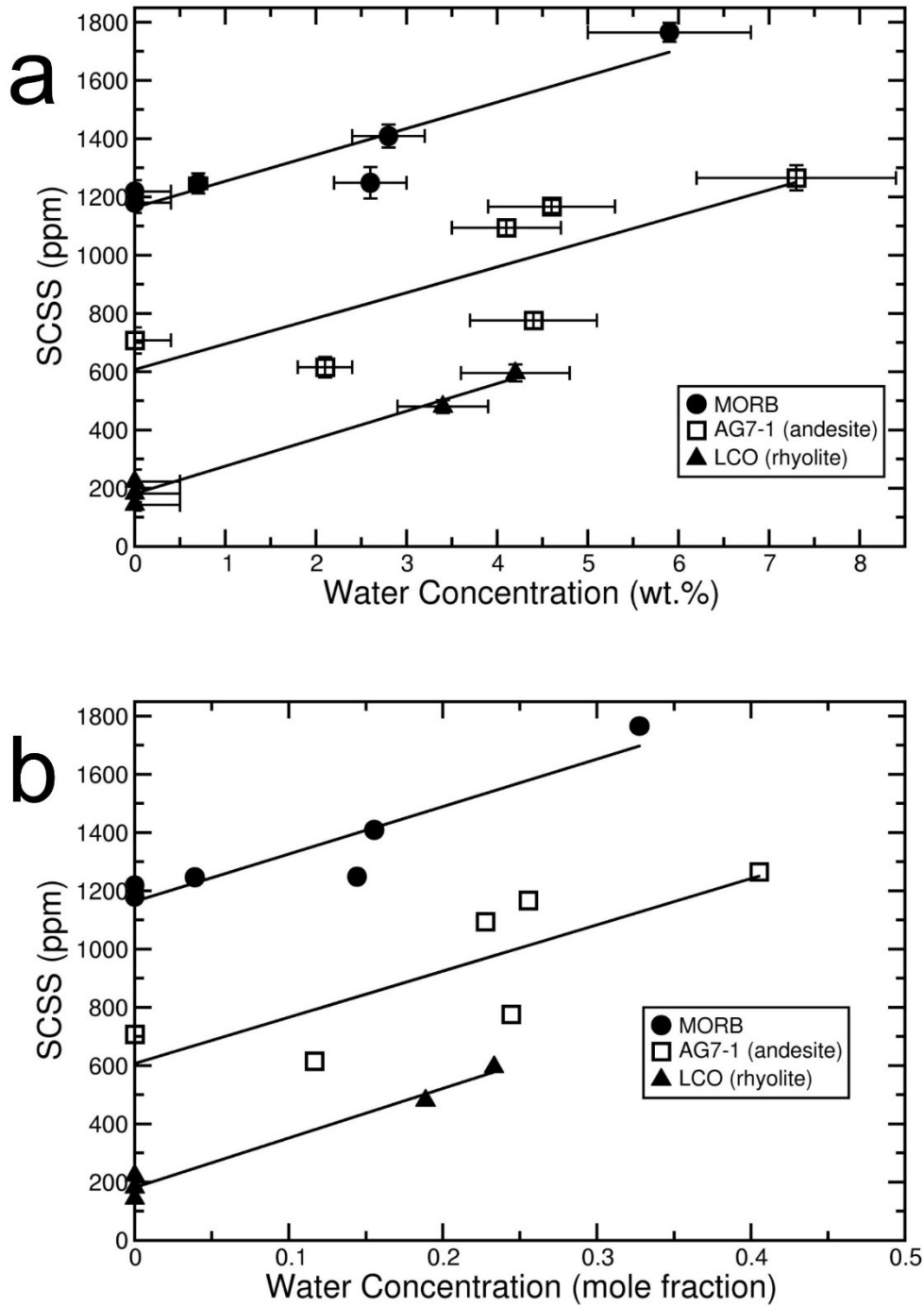


Figure 4: The sulphur concentration at sulphide saturation in the silicate melts of our experiments, measured by electron microprobe as a function of the total melt water concentration, measured by Raman spectroscopy (a) in wt.%, and (b) in mole fraction.

Chapter 4: Discussion

On average, we note good agreement between our anhydrous experiments and those of Liu et al. (2007) for compositions MORB (this study: 1218 ± 40 ppm, Liu et al.: 1214 ± 29 ppm) AG7-1 andesite (this study: 707 ± 45 ppm, Liu et al.: 725 ± 22 ppm), and LCO rhyolite (this study: 181 ± 32 ppm, Liu et al.: 157 ± 14 ppm). However, the Etna basalt composition shows significant discrepancies between our measurements and Liu et al. (2007)'s. Liu et al. (2007) report SCSS values decreasing from 1417 ± 104 to 663 ± 112 ppm with water content increasing from anhydrous to 4.0 wt.% for their experiments of Etna compositions at 1250 °C, 1 GPa, oxygen fugacities at or near the CCO buffer. For the same conditions and composition, we find the SCSS to increase from 865 ± 47 to 1084 ± 47 for water concentrations increasing from anhydrous to 5.5 wt.%. We have tried reconciling our Etna data with Liu et al. (2007)'s by analysing the water concentration of their hydrous Etna experiments by Raman. These were found to be close to anhydrous, despite the reported water concentrations as high as 4.0 wt.%. Even with water concentrations near anhydrous, the results of these experiments are not in agreement

with those of this study. We do not believe a defective temperature control was at fault in our experiments, as all of our Etna-composition experiments were run simultaneously with a matching MORB-composition and the SCSS of our MORB and those of Liu et al. (2007)'s are equal within uncertainty. Because of the discrepancies between our results on Etna basalt and those of Liu et al. (2007), and because our MORB experiments already provided data for basaltic compositions, we chose not to include the results from our Etna experiments into our modelling, focusing instead on our three other compositions.

Effect of water on the SCSS

The impact of water on the structure of silicate melts, and on their properties is well-known, but poorly understood. It is still debated what mechanisms control the effect of water on melts. Water is dissolved in melts as both OH⁻ and molecular H₂O species, and their relative abundance is a complex function of at least temperature and melt composition (e.g., Stolper, 1982; Burnham, 1994; Liu et al., 2005). However, the exact

mechanism of dissolution of water in melts still demands further studies (e.g., Mysen & Richet, 2005).

The positive correlation that we observe between the SCSS and water concentration in the melt (see Figure 4) is in contradiction with the findings of Liu et al. (2007), who found a negative relationship in basaltic melts (see Figure 1), and a slight positive trend in rhyolitic melts. Similarly, the thermodynamic model of Moretti et al. (2003) for sulphur phases in C-O-H-S systems predicts a decrease in the sulphur concentration as melts become more hydrous. They note, however, that the presence of additional S-bearing phases (e.g., crystalline pyrrhotite) could potentially lead to significant changes of the partitioning of S between the different phases. More recently, Moune et al. (2009) also found that an increase in melt water concentration resulted in an increase in the SCSS of their experiments. They attributed this behavior to the depolymerising nature of water in silicate melts, resulting in a higher SCSS.

Factors controlling the SCSS

Both the effect of temperature and the effect of pressure on the SCSS have been extensively studied and documented. All previous studies agree that temperature has a positive effect on the SCSS, and most studies agree that pressure has a slight negative effect over a large pressure range (e.g., Wendlandt, 1982; Mavrogenes & O'Neill, 1999; Holzheid & Grove, 2002), or no measurable effect over smaller pressure variations, such as 0.5 to 1 GPa (e.g., Carroll & Rutherford, 1985; Liu et al., 2007).

The oxygen fugacity of the system is also an important factor in controlling the SCSS, but changes at low oxygen fugacity result in less direct changes in the SCSS than temperature or pressure because they act by affecting the composition of the sulphide phase (e.g., Fincham & Richardson, 1954; Haughton et al., 1974; Katsura & Nagashima, 1974; Carroll & Rutherford, 1985; Rutherford & Devine, 1996; Mavrogenes & O'Neill, 1999; O'Neill & Mavrogenes, 2002; Liu et al., 2007). However, an increase of the oxygen fugacity to about 1.5 log units above the NNO buffer leads to a greater S^{6+}/S^{2-} ratio in the melt and the dominant sulphur species changes from sulphide to

sulphate (e.g., Fincham & Richardson, 1954; Carroll & Rutherford, 1985, 1987; Wallace & Carmichael, 1992; Wilke et al., 2008). Sulphur saturation is then expressed as the sulphur concentration at anhydrite saturation, SCAS (e.g., Baker & Moretti, 2011).

The melt composition has an important effect on the SCSS (e.g., Haughton et al., 1974; Carroll & Rutherford, 1985, 1987; Moretti & Ottonello, 2005; Liu et al., 2007; this study).

Further, the SCSS is closely related to the concentration of FeO in the melt (e.g., Haughton et al., 1974; Poulson & Ohmoto, 1990; Wallace & Carmichael, 1992). This is because of all the major network modifying cations present in silicate melts (i.e., Mg, Ca, Fe, Na, K), Fe²⁺ favors bonding with S²⁻ the most (Fyfe, 1964). However, because the activity of Fe²⁺ is itself a complex function of other factors in the melt, other cation-sulphide melt species are possible (Moretti & Ottonello, 2003, 2005); the SCSS is not only affected by the FeO concentration of the melt, but also by the presence of other elements (Eissa et al., 1996; O'Neill & Mavrogenes, 2002). Mafic melts have higher SCSS values than their silicic counterparts partly because they are richer in non-bridging oxygens, which depolymerise the melt and allow sulphur to replace free

oxygens and be dissolved in greater quantities (Fincham & Richardson, 1954).

Furthermore, Haughton et al. (1974) and O'Neil & Mavrogenes (2002) have

demonstrated the major effect of FeO on the SCSS in basaltic melts.

Chapter 5: Modelling the SCSS

There are two main approaches to modelling the SCSS, thermodynamically rigorous models (e.g., Moretti et al., 2003), and thermodynamically based, but empirical models.

Empirical models are separated into three schools of thought when it comes to the characterisation of the melt composition. One uses the NBO/T ratio (e.g., Holzheid & Grove, 2002), while another approach is to simply use the mole fraction of oxides that are found to have a statistically significant effect on the SCSS (e.g., Li & Ripley, 2009), and the last is to use a predetermined, systematic parameter, like the MFM to describe melt composition (refer to equation 5; e.g. Liu et al., 2007). For our modelling, we favoured the latter two approaches, as their necessary parameters are completely defined. Thus, we chose to build two different models, similar to the models of Liu et al. (2007) and of Li & Ripley (2009).

Model A (MFM)

The model of Liu et al. (2007) for sulphide saturation is thermodynamically motivated by equation 4, and is of the form:

$$\ln(S) = \mathbf{a} + \frac{\mathbf{b}}{T} + \mathbf{c} \frac{P}{T} + \mathbf{d} \ln(MFM) + \mathbf{e} MFM XH_2O + \mathbf{f} \ln(XH_2O) + \mathbf{g} XFeO \quad (7)$$

where S is the SCSS in ppm, T is the temperature in Kelvin, P is the pressure in GPa, MFM is the modified FM parameter as defined in equation 5, X are mole fractions, and \mathbf{a} , \mathbf{b} , \mathbf{c} , \mathbf{d} , \mathbf{e} , \mathbf{f} , and \mathbf{g} are fitting constants. The 'a' term is related to the entropy, the 'b' term is associated with the enthalpy, the 'c' term is related to the change in volume, and the other terms are linked to the equilibrium constant of reaction 4. Liu et al. (2007) fit their model using values from their own experiments as well as values from the literature, totaling 117 analyses of silicate melts at sulphide saturation, 29 of which were hydrous. While the model is based on the dissolution of iron sulphide into the melt (see equation 4), the addition of the ' $\ln(XH_2O)$ ', and ' $MFM * XH_2O$ ' terms have no theoretical foundation, and were added to provide a better fit to their calibration dataset. In our study, we did not find the addition of those terms to significantly improve the fit between measured and calculated SCSS values, and therefore we chose not to use these two terms. Instead, we chose to incorporate water in our models as a simple ' XH_2O ' term, the total water in the melt; this term is similar to that used by Li & Ripley (2009). This term is also

devoid of any theoretical foundation and does not distinguish between the different water species present in the melt, but we empirically demonstrated that total water affects the SCSS linearly (see Figure 4).

The reasoning behind our choice is twofold: (1) it simplifies the application of the model where spectroscopic measurements are not available to discriminate between OH⁻ and molecular H₂O species, and (2) it is the simplest way to adequately quantify the effect of water, without risking overfitting of the data. Therefore, we update the form of Liu et al. (2007)'s model to our own Model A:

$$\ln(S, ppm) = a + \frac{b}{T} + c \frac{P}{T} + d \ln(MFM) + e XFeO + f XH_2O \quad (8)$$

Model B (mole fractions of oxides):

Li & Ripley (2009) did not conduct any experiments, but instead used a total of 205 sulphide-liquid saturated experiments from various sources to calibrate their equation and found that SiO₂, TiO₂, FeO, CaO, and H₂O were the only oxides that contributed significantly to their SCSS model for their dataset. Their model is of the form:

$$\ln(X_S) = a + \frac{b}{T} + c P + d XH_2O + e XSiO_2 + f XTiO_2 + g XFeO + h XCaO \quad (9)$$

where X are mole fractions, a , b , c , d , e , f , g , and h are constants, T is the temperature in Kelvin, and P is the pressure in kbars. For our own model, we chose to use pressures in GPa divided by the temperature in Kelvin for consistency with Model A of our study. We also opted to calculate the SCSS as S in ppm, and not as mole fraction. We found a larger number of significant oxides for modelling the SCSS than Li & Ripley (2009). We found that SiO_2 , TiO_2 , FeO , MgO , CaO , Na_2O , K_2O , and H_2O all play a significant role in determining the SCSS. This is in partial agreement with the previous studies of Haughton et al. (1974), Wallace & Carmichael (1992), and Li & Ripley (2009), who had found that different combinations of these elements significantly impacted the SCSS. Interestingly, we found that the same oxides as used by Ariskin et al. (2013) significantly affected the SCSS (i.e., SiO_2 , TiO_2 , Al_2O_3 , FeO , MgO , CaO , Na_2O , and K_2O). However, and as opposed to Ariskin et al. (2013), we included the effect of water in our model. We therefore update the form of the Li & Ripley (2009) model to our own Model B:

$$\ln(S, ppm) = a + \frac{b}{T} + c \frac{P}{T} + f XH_2O + g XSiO_2 + h XTiO_2 + i XAl_2O_3 + j XFeO + k XMgO + l XCaO + m XNa_2O + n XK_2O \quad (10)$$

Model calibration

In our goal of creating a model applicable to a wide range of conditions, and because we designed our own experiments to investigate the effect of water only, we compiled and used 220 experiments, 21 of which are hydrous experiments, in order to calibrate our models. These were carefully selected measurements in the literature from previous studies of sulphide solubility, the SCSS, and of partitioning in sulphide-saturated systems. Combined with our experimental data, we assembled a total of 238 sulphide-saturated glasses, including 34 hydrous experiments in which water concentration in the melt was directly measured using methods such as Fourier-transform infrared spectroscopy, Raman spectroscopy, SIMS, or Karl-Fischer titration. For pressures of 1 atm, we used the dataset of the “Series I” experiments of Haughton et al. (1974). We discarded experiments 15 F2, 19 F2, 20 F2, or 21 F2 because of their high FeO concentrations that are not applicable to natural basalts (>35 wt.%). Additionally, we did not use run numbers 4 DF 2, 7 DF 2, or 7 F2 because of the self-consistency issues raised by O’Neill & Mavrogenes (2002). For similar reasons, brought up by O’Neill &

Mavrogenes (2002), we did not use the dataset of Buchanan et al. (1983). We complemented these data with analyses of silicate glasses saturated with sulfides from the publications of Peach & Mathez (1993), Peach et al. (1994), Mavrogenes & O'Neill (1999), Baker et al., (2001), Holzheid & Grove (2002), Sattari et al. (2002), Jugo et al. (2005), Liu et al. (2007), Brenan (2008), Moune et al. (2009), Righter et al., (2009), Beermann et al. (2011), and Ding et al. (2014). We report our full dataset used for calibration in Appendix I. The calibration dataset includes Martian basaltic compositions, and terrestrial compositions ranging from basaltic to rhyolitic.

We did not use the Etna experiments of Liu et al. (2007) because of discrepancies between our measurements and theirs. Additionally, we chose not to use data from hydrous studies that did not directly characterise their melt water concentrations in quenched glasses using methods such as Fourier-transform infrared spectroscopy, Raman, SIMS, or Karl-Fischer titration. This criterion excludes some or all of the hydrous glasses from Luhr (1990), Clemente et al. (2004), Liu et al. (2007), Beermann

et al. (2011), Zajacz et al. (2013), Jago & Dasgupta (2013), and Ding et al. (2014) from the calibration dataset.

Other studies of sulphide saturated silicate melts exist in the literature, but we chose not to use their results because (1) the authors did not report the full melt compositions (i.e., Shima & Naldrett, 1975; Danckwerth et al., 1979; Wendlandt, 1982), (2) the systems investigated are far in composition from natural systems (i.e., Buchanan & Nolan, 1979; Gaetani & Grove, 1997; O'Neill & Mavrogenes, 2002), or (3) their results were inconsistent with other studies such as showing a negative effect of temperature on the SCSS (i.e., Bockrath et al., 2004; Tsujimara & Kitakaze, 2005).

By fitting the data using non-linear regression in the software NCSS 2004 (Hintze, 2004), we find the fitting coefficients that we report in Table 4, along with their standard error. Note that the digits do not represent precision, but instead we purposely retained them to avoid rounding errors. The R-squared value for Model A is 0.804, while for Model B it is 0.932. The standard errors of the coefficients are less than 20% relative for both models. Because the models are calibrated using a dataset of a wide variety of

Table 4: Fitting parameter coefficients for the characterisation of the SCSS

Term	Model A (MFM)*		Model B (XOxides)†		
	Value	Standard Error	Value	Standard Error	
a	Constant	10.269	0.424	49.478	4.480
b	1/T	-4692.6	533.0	-5849.7	370.0
c	P/T	-332.68	54.47	-325.37	33.38
d	ln(MFM)	0.46591	0.03882		
e	ln(XFeO)	0.31030	0.03632		
f	XH ₂ O	3.7894	0.5701	-35.583	4.536
g	XSiO ₂			-40.365	4.472
h	XTiO ₂			-35.494	5.142
i	XAl ₂ O ₃			-39.202	3.950
j	XFeO			-34.217	4.786
k	XMgO			-36.963	4.412
l	XCaO			-36.335	4.709
m	XNa ₂ O			-35.641	5.056
n	XK ₂ O			-46.392	5.018

We report more digits than are significant to avoid rounding errors.

*For the equation of the form:

$$\ln(S, ppm) = \mathbf{a} + \frac{\mathbf{b}}{T} + \mathbf{c} \frac{P}{T} + \mathbf{d} \ln(MFM) + \mathbf{e} XFeO + \mathbf{f} XH_2O$$

†For the equation of the form:

$$\ln(S, ppm) = \mathbf{a} + \frac{\mathbf{b}}{T} + \mathbf{c} \frac{P}{T} + \mathbf{f} XH_2O + \mathbf{g} XSiO_2 + \mathbf{h} XTiO_2 + \mathbf{i} XAl_2O_3 + \mathbf{j} XFeO + \mathbf{k} XMgO \\ + \mathbf{l} XCaO + \mathbf{m} XNa_2O + \mathbf{n} XK_2O$$

conditions, they are applicable to Martian basaltic and terrestrial basaltic to rhyolitic melts at pressures from 1 atm to 5 GPa, temperatures from 1050 to 1800 °C, melt water concentrations from anhydrous to 7.3 wt.%, and oxygen fugacities less than about 1.5 log unit below the NNO oxygen buffer (Frost, 1991), where sulphide predominates (Wilkes et al., 2011).

Figure 5 shows the comparison between the measured SCSS and the SCSS calculated by both our models. The accuracy of our models can be evaluated by the average squared deviation between the calculated and measured values, as well as with the χ^2 value, defined as:

$$\chi^2 = \sum \frac{(SCSS_{calc} - SCSS_{meas})^2}{SCSS_{meas}} \quad (11)$$

Model A yields an average squared deviation of 0.11, and a χ^2 value of 3.77 for the 238 samples used for calibration. Model B produces an average squared deviation of 0.04, and a χ^2 value of 1.30.

Additionally, we randomly selected 14 measurements from the dataset of this study to build a dataset to independently test our models. This dataset was not used in

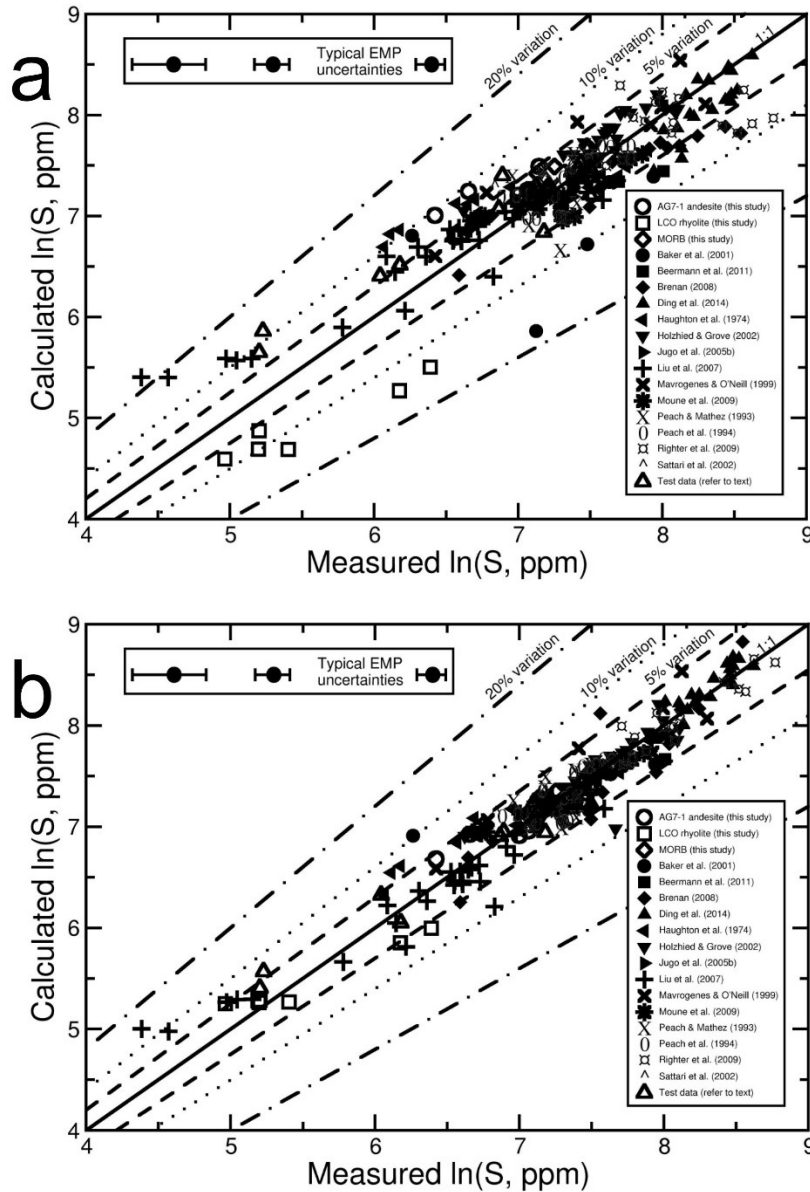


Figure 5: The calculated and measured SCSS for the sets of experiments used for calibrating (a) Model A, and (b) Model B. A perfect agreement between the model and the data would have all the points plotting on the 1:1, full line. The dashed line shows a relative variation of 5% from ideality, the dotted line shows a relative variation of 10%, and the dot-dashed line shows a relative variation of 20%. Model A (a) shows good agreement with the data to within about 10%, relative and Model B (b) reproduces the data to within about 5% relative.

calibrating the equations and it is therefore a more rigorous way of testing the model than the goodness of fit parameters. The 14-member test dataset is comprised of experiments from Haughton et al. (1974), Peach & Mathez (1993), Peach et al. (1994), Mavrogenes & O'Neill (1999), Sattari et al. (2002), Holzheid & Grove (2002), Jugo et al. (2005), Liu et al. (2007), Brenan (2008), Richter et al. (2009), and Moune et al. (2009). The test dataset spans SiO₂ concentrations from 44.7 to 77.9 wt.%. We report the full dataset used for testing in Appendix II. We also plot the test data in Figure 5. In Model A, the SCSS of most studies is successfully calculated to within about 10% relative, including the test dataset. Model B reproduces the SCSS of most studies to within about 5% relative, including the test dataset. We note however that both models have their greatest weaknesses in reproducing the measured SCSS of low-SCSS, high-silica samples.

As pointed out by Koptev-Dvornikov et al. (2012), logarithmic scales, like the one we used for modelling the SCSS, are not desirable when comparing relative goodness of fit. For this reason, we re-plot our results in Figure 6 as the difference between the

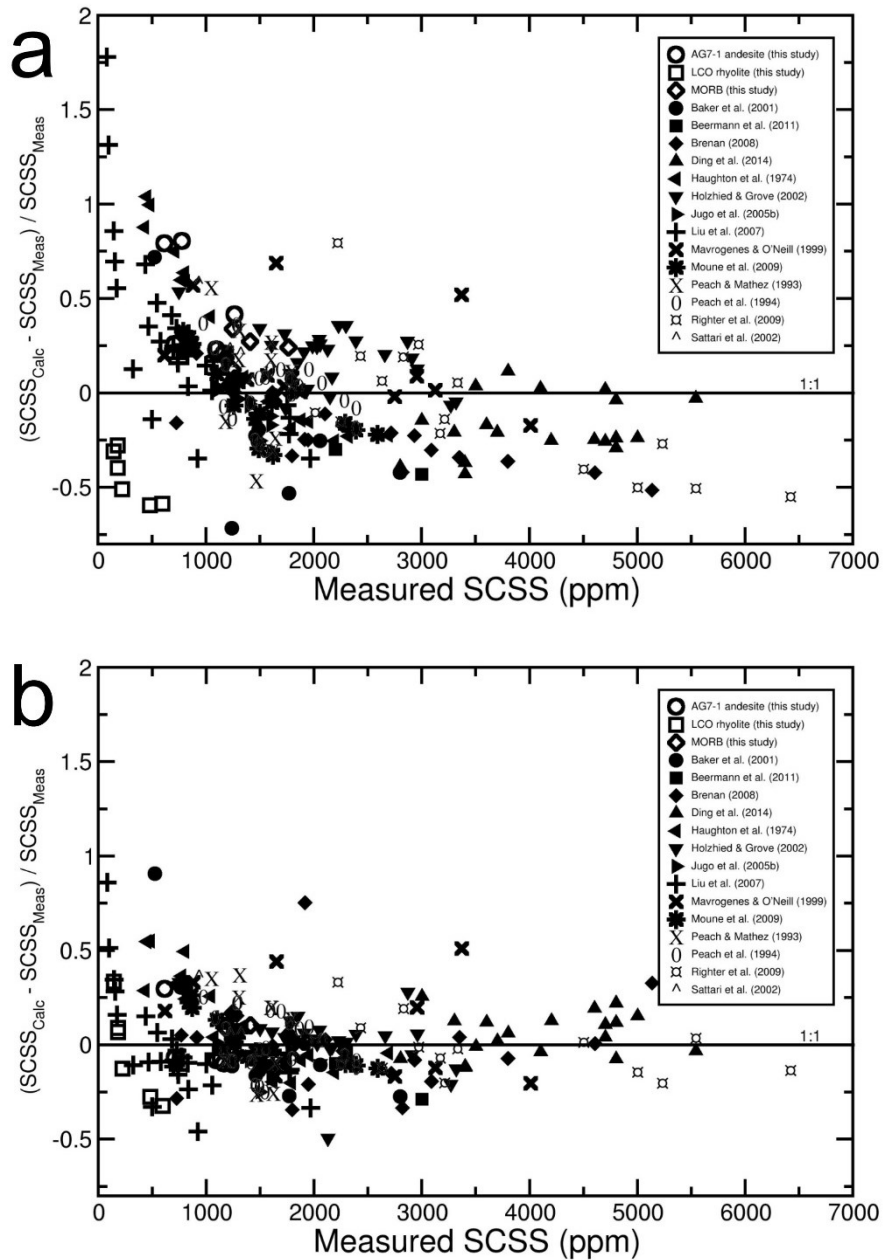


Figure 6: The difference between the calculated and the measured SCSS divided by the measured against the measured SCSS. This shows how the relative difference between our modelled, predicted values, and the measured values vary as a function of the total sulphur concentration of the melt. As expected, both Model A (a) and Model B (b) show greater scatter at low SCSS, in more silicic melt compositions.

calculated SCSS and the measured SCSS divided by the measured SCSS as a function of the measured SCSS, or $(SCSS_{calc}-SCSS_{meas})/SCSS_{meas}$ vs. $SCSS_{meas}$. This shows the relative difference between our modelled values and the measured values and how it varies as a function of the total sulphur.

We favour Model B to Model A because of its better reproducibility of both the calibration dataset and the test dataset. We note however that Model B does not take into consideration the oxygen fugacity of the system, while Model A does, meaning that the effect of oxygen fugacity is not considered in the model that fits best. We suggest that this is due to the various sulphur and water species that predominate in the melt at different oxygen fugacities that are too complex for our simplistic Model A approach to predict. On the other hand, Model B averages out their complex behaviours, giving a better representation of the SCSS over a wider range of conditions.

Modelled effect of water on the SCSS

Our favoured model, Model B, demonstrates an increase in the SCSS with increasing melt water concentration, as shown in Figure 7. The basaltic composition of MAF-9

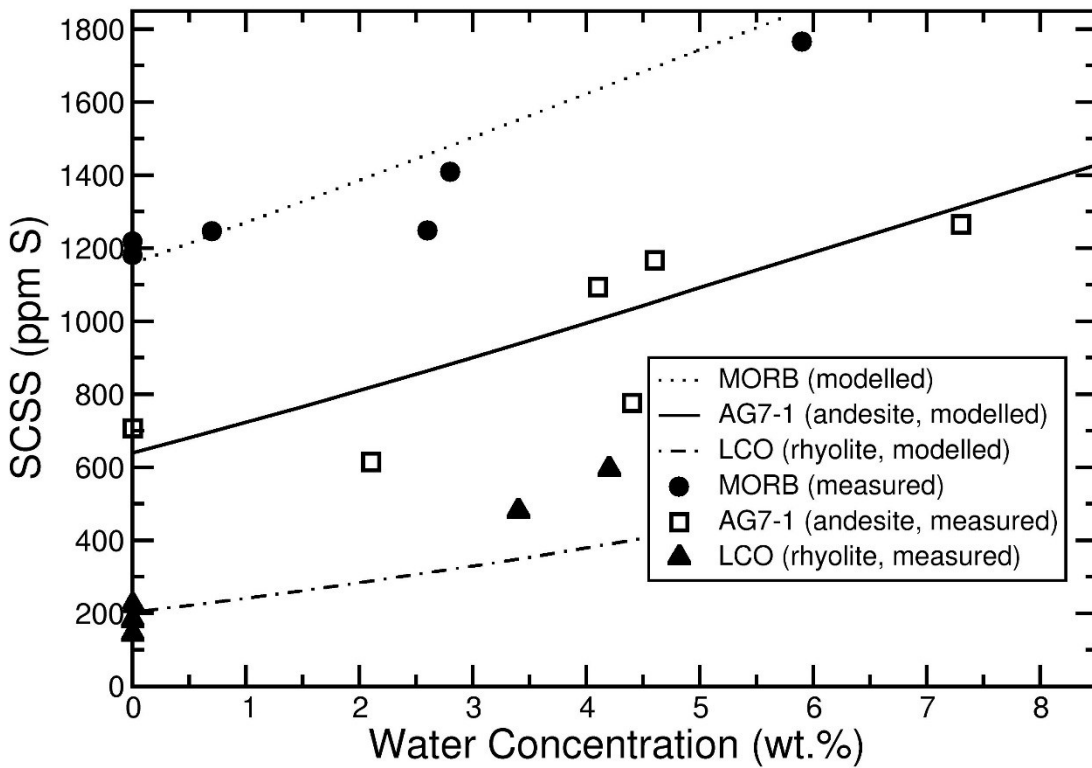


Figure 7: The effect of water on the SCSS as calculated using Model B. The dotted line represents a melt of basaltic composition (MAF-9), the solid line is for a melt of andesitic composition (MAF-36), and the dotted-dashed line shows a melt of rhyolitic composition (MAF-39). Also plotted are our experimental results of MORB (filled circle), AG7-1 (opened square), and LCO (filled triangle). All three compositions show an increase in the SCSS with increasing total dissolved water.

(dotted line) shows an increase of about 120 ppm S per wt.% of added dissolved water, the andesitic composition of MAF-36 (full line), about 90 ppm per wt.% added water, and the rhyolitic composition of MAF-39 (dotted-dashed line), about 45 ppm per wt.% added water. These values are similar to what we measured experimentally for the compositions used in this study. This means that an ascending, degassing magma that is losing dissolved water will see its SCSS decrease, possibly leading to the generation of a separate sulphide phase.

Chapter 6: Applications

Application to hydrous, experimental melts

Our calibration dataset is scarce at low SCSS conditions, commonly associated with silica-rich melts. These are the compositions that our model has the greatest difficulty replicating. In Figure 8, we plot the results from Model B for hydrous SCSS measurements that were not included in the calibration dataset because their water concentrations were determined indirectly (i.e., Luhr, 1990; Clemente et al., 2004; Liu et al., 2007; Beermann et al., 2011; Zajacz et al., 2013; Jago & Dasgupta, 2013; Ding et al., 2014). We report this dataset in Appendix III. We did not include the experiments of Clemente et al. (2004) that contained more molecular sulphur than FeO, because such melts do not appear to occur in igneous systems. The vast majority of these measurements plot in the low-SCSS region, where our calibration dataset is scarce. Even without direct water concentration measurements, we note that Model B reproduces most of the data to within about 20% relative.

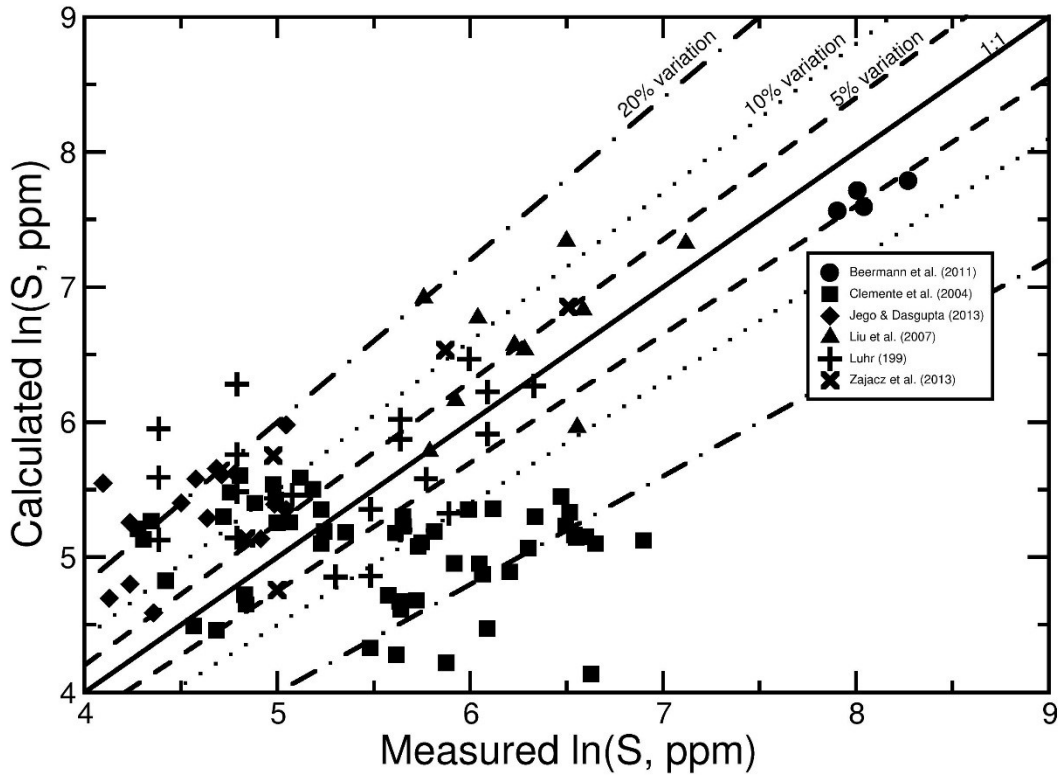


Figure 8: The SCSS calculated from our Model B against the measured SCSS for the hydrous experiments not used in developing the model because their water concentrations were determined indirectly. A perfect agreement between the model and the data would have all the points plotting on the 1:1, full line. The dashed line shows a relative variation of 5% from ideality, the dotted line shows a relative variation of 10%, and the dot-dashed line shows a relative variation of 20%. Most measurements are silicic in compositions and are reproduced to about 20% relative variation (within the dotted-dashed lines).

Application to hydrous, Ni-rich natural melts

A thought-provoking paper by Ariskin et al. (2013) studied the effect of Ni on the SCSS in mostly anhydrous silicate melts, without studying the effect of water. Their model is based upon the idea that positively-charged Fe-Ni sulphide complexes (e.g., $(\text{Fe}_y\text{Ni}_{1-y})_z\text{S}^{2(z-1)+}$) are present in the melt, and play an important role on the SCSS. Our model does not consider the effect of Ni, but the calibration dataset does contain SCSS measurements from Ni partitioning studies (i.e., Peach & Mathez, 1993; Sattari et al., 2002), with Ni concentrations in the melt reaching 240 ppm. Our model reproduces the SCSS of these Ni-rich datasets within 5% relative; less than the uncertainty in the measurements. Ariskin et al. (2013) looked at a set of 41 hydrous, natural basalt samples from pillow rim glasses in the Siqueiros fault zone in the East Pacific Rise (e.g., Danyushesvky et al., 2003), with Ni concentrations ranging from 36.9 to 222.6 ppm. These glasses cover a large range of compositions from primitive to highly evolved basaltic melts, and 39 of the 41 glasses analysed contained a distinctive immiscible sulphide phase. Quenched sulphides as inclusions in olivine phenocrysts were also

noted. Accounting for the water concentrations of these samples, they modeled the crystallization temperatures of the Siqueiros fault zone samples to range from 1110 to 1235 °C. Adding to this dataset, Ariskin et al. (2013) included 24 analyses from pillow rims collected in ODP hole 896A (e.g., Danyushevsky et al., 2002). These glasses have Ni concentrations ranging from 90.5 to 174.4 ppm, and all contained sulphide blebs, demonstrating their saturation with sulphides. They calculated the temperatures to be between 1180 and 1210°C. Figure 9 compares the measured SCSS with the SCSS predicted by our Model B, assuming an oxygen fugacity of FMQ, and a pressure of 0.05 GPa, as used by Ariskin et al. (2013). Our Model B reproduces the SCSS of the natural glasses within about 5% relative, or below the uncertainty of the measurements. We note however, that the SCSS values calculated by our model are skewed towards higher values than the measurements. The glasses with the higher Ni concentrations are more overestimated by our model than those with lower Ni concentrations, while still being approximated to within about 5% relative by our model.

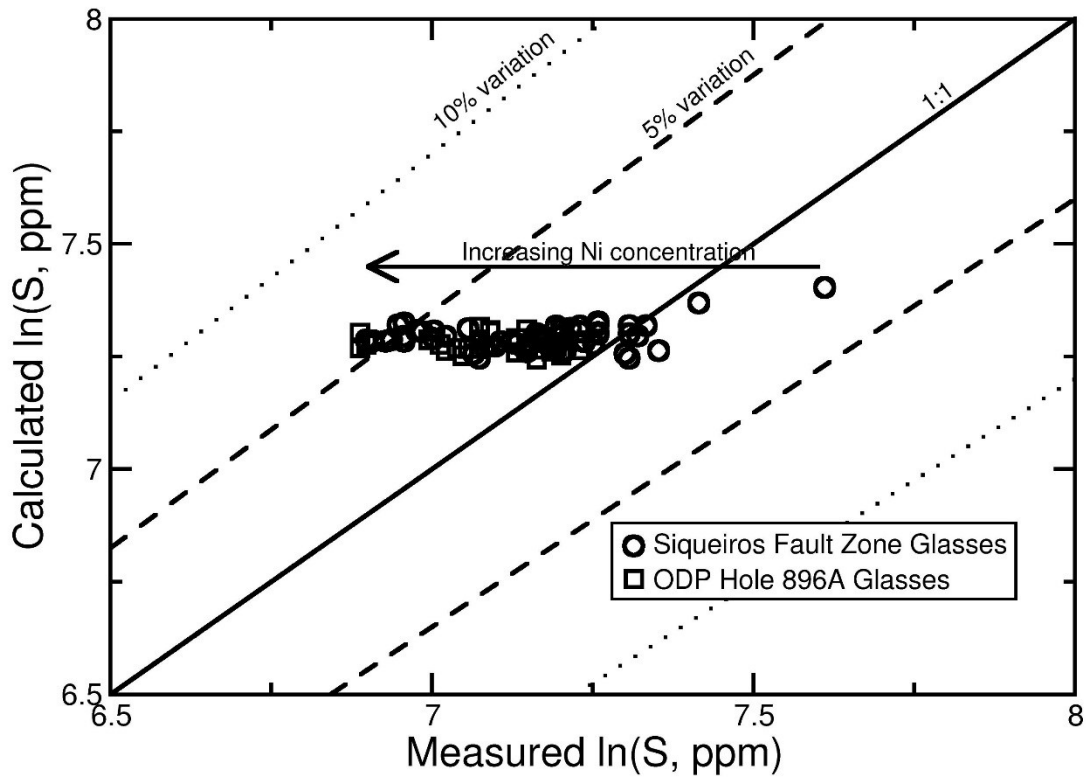


Figure 9: The SCSS calculated from our Model B against the measured SCSS for the hydrous, Ni-rich natural glass measurements of Ariskin et al. (2013). A perfect agreement between the model and the data would have all the points plotting on the 1:1, full line. The dashed line shows a relative variation of 5% from ideality, the dotted line shows a relative variation of 10%, and the dot-dashed line shows a relative variation of 20%. Most measurements are reproduced to about 5% relative variation (dashed lines). The arrow shows the trend of increasing Ni concentration in the glasses.

We suggest that while there may indeed be a correlation between the Ni concentration in the melt and the SCSS as would be predicted from basic thermodynamics, because our model reproduces the SCSS to a precision of about 5% relative, there is no need for a more complicated multi species FeNiS model to determine the SCSS, even in natural samples.

Chapter 7: Conclusions

Our experiments and our findings on the effect of water on the SCSS demonstrate clearly for the first time that magmas with larger concentrations of water are able to dissolve a larger amount of sulphur before reaching sulphide saturation (about 100 ppm of S per wt.% of added dissolved water for basalts). This means that as a parcel of magma rises through the crust, degasses and becomes less hydrous, its sulphide saturation will decrease and potentially lead to the generation of an immiscible sulphide phase.

In conclusion, we have improved on the previous models for predicting the sulphur concentration at sulphide saturation in natural silicate melts with our contribution of hydrous experiments. Further, we have shown that while Ni appears to positively influence the SCSS, its effect does not seem to be significant, as it is less than the uncertainty of the SCSS measurements. While constructing our calibration dataset, we noticed a lack of low SCSS, high silica data, both anhydrous and hydrous with directly quantified total water concentrations in the literature. Future work should be focused on

filling this gap. Moreover, future work specifically on the hydrous SCSS should be concerned with spectroscopic studies to characterise the different sulphur and water species that dominate in a silicate melt as a function of water concentration and oxygen fugacity.

REFERENCES

- Ariskin A.A., Danyushevsky L.V., Bychkov K.A., McNeill A.W., Barmina G.S., Nikolaev G.S. (2013) Modeling solubility of Fe-Ni sulfides in basaltic magmas: the effect of nickel. *Econ. Geol.* **108**, 1983-2003.
- Baker D.R. (1991) Interdiffusion of hydrous dacitic and rhyolitic melts and the efficacy of rhyolite contamination by dacitic enclaves. *Contrib. Mineral. Petrol.* **106**, 462-473.
- Baker D.R., Barnes S.J., Simon G., Bernier F. (2001) Fluid transport of sulfur and metals between sulfide melt and basaltic melt. *Can. Mineral.* **39**, 537-546.
- Baker D.R. (2004) Piston-cylinder calibration at 400 to 500 MPa, a comparison of using water solubility in albite melt and NaCl melting. *Am. Mineral.* **89**, 1553-1556.
- Baker D.R. & Moretti R. (2011) Modeling the solubility of sulfur in magmas: a 50-year old geochemical challenge. In *Sulfur in Magmas and Melts and its Importance for Natural and Technical Processes* (eds. H. Behrens and J.D. Webster). Mineral Society of America, Reviews in Mineralogy **73**, pp. 167-213.
- Beermann O., Borcharnikov R.E., Holtz F., Diedrich O., Nowak M. (2011) Temperature dependence of sulfide and sulfate solubility in olivine-saturated basaltic magmas. *Geochim. Cosmochim. Acta* **75**, 7612-7631.

- Behrens H., Roux J., Neuville D.R., Siemann M. (2006) Quantification of dissolved H₂O in silicate glasses using confocal microRaman spectroscopy. *Chem. Geol.* **229**, 96-112.
- Behrens H. & Webster J.D. (2011) Studies of sulfur in melts – motivations and overview. In *Sulfur in Magmas and Melts and its Importance for Natural and Technical Processes* (eds. H. Behrens and J.D. Webster). Mineral Society of America, Reviews in Mineralogy **73**, pp. 1-8.
- Bockrath C., Ballhaus C. and Holzheid A. (2004) Stabilities of laurite RuS₂ and monosulfide liquid solution at magmatic temperature. *Chem. Geol.* **208**, 265-271.
- Brenan J.M. (2008) Re-Os fractionation by sulfide melt-silicate melt partitioning: a new spin. *Chem. Geol.* **248**, 140-165.
- Buchanan D.L., Nolan J., Wilkinson N. and de Villiers J.R. (1983) An experimental investigation of sulphur solubility as a function of temperature in synthetic silicate melts. *Geol. Soc. South Africa Spec. Pub* **7**, 383-391.
- Burnham, C.W. (1994) Development of the Burnham model for prediction of H₂O solubility in magmas. In *Volatiles in Magmas* (eds. M.R. Carroll and J.R. Holloway). Mineral Society of America, Reviews in Mineralogy **30**, pp. 123-129.
- Carroll M.R. & Rutherford M.J. (1985) Sulfide and sulfate saturation in hydrous silicate melts. *J. Geophys. Research* **90**, 601-612.

- Carroll M.R. & Rutherford M.J. (1987) The stability of igneous anhydrite: Experimental results and implications for sulfur behavior in the 1982 El Chichon trachyandesite and other evolved magmas. *J. Petrol.* **28**, 781-801.
- Charbiron A., Pironon J., Massare D. (2004) Characterization of water in synthetic rhyolitic glasses and natural melt inclusion by Raman spectroscopy. *Contrib. Mineral. Petrol.* **146**, 485-492.
- Clemente B., Scaillet B. and Pichavant M. (2004) The solubility of sulfur in hydrous rhyolitic melts. *J. Petrol.* **45**, 2171-2196.
- Danckwerth P.A., Hess P.C. and Rutherford M.J. (1979) The solubility of sulfur in high-TiO₂ mare basalts. *Proc. 10th Lunar Planet. Sci. Conf.*, 517-530.
- Danyushevsky L.V., McNeill A.W., Sobolev A.V. (2002) Experimental and petrological studies of melt inclusions in phenocrysts from mantle-derived magmas: an overview of techniques, advantages and complications. *Chem. Geol.* **183**, 5-24.
- Danyushevsky L.V., Perfit M.R., Eggins S.M., Falloon T.J. (2003) Crustal origin for coupled ultra-depleted and "plagioclase" signatures in MORB olivine-hosted melt inclusions: evidence from the Siqueiros transform fault, East Pacific Rise. *Contrib. Mineral. Petrol.* **114**, 619-637.

- Ding S., Dasgupta R., Tsuno K. (2014) Sulfur concentration of martian basalts at sulfide saturation at high pressures and temperatures – implications for deep sulfur cycle on Mars. *Geochim. Cosmochim. Acta* **131**, 227-246.
- De Hoog J.M., Mason P.D. and Van Bergen M.J. (2001) Sulfur and chalcophile elements in subduction zones: constraints from a laser ablation ICP-MS study of melt inclusions from Galunggung Volcano, Indonesia. *Geochim. Cosmochim. Acta* **65**, 3147-3164.
- Devine J., Gardner J.E., Brack H., Layne G.D., Rutherford M.J. (1995) Comparison of microanalytical methods for estimating H₂O contents of silicic volcanic glasses. *Am. Mineral.* **80**, 319-328.
- Eissa M.M., Elfawakhry K.A., Taylor W., Elfaramawy H. and Ahmed A.M. (1996) Ferrous oxide activity in FeO-TiO₂-CaO-Al₂O₃ system. *ISIJ International* **36**, 512-516.
- Fincham C.J.B. & Richardson F.D. (1954) The behavior of sulfur in silicate and aluminate melts. *Proc. Roy. Soc. London* **223A**, 40-61.
- Frost B.R. (1991) Introduction to oxygen fugacity and its petrologic importance. In *Oxide Minerals: Petrologic and Magnetic Significance* (ed. D.H. Lindsley). Mineralogical Society of America, Reviews in Mineralogy **25**, pp. 1-9.
- Fyfe W.S. (1964) *Geochemistry of solids: An Introduction*. McGraw-Hill Inc., New York.

- Gaetani G.A., Grove T.L. (1997) Partitioning of moderately siderophile elements among olivine, silicate melt, and sulfide melt: constraints on core formation in the Earth and Mars. *Geochim. Cosmochim. Acta* **61**, 1829-1846.
- Harrison T.M., Watson, E.B. (1983) Kinetics of zircon dissolution and zirconium diffusion in granitic melts of variable water content. *Contrib. Mineral. Petrol.* **84**, 66-72.
- Haughton D.R., Roeder P.L. and Skinner B.J. (1974) Solubility of sulfur in mafic magmas. *Econ. Geol.* **69**, 451-467.
- Hintze J. (2004) NCSS 2004. NCSS, LLC. Keyserville, Utah, USA.
- Holzheid A. & Grove T.L. (2002) Sulfur saturation limits in silicate melts and their implications for core formation scenarios for terrestrial planets. *Am. Mineral.* **87**, 227-237.
- Jakobsson S. & Oskarsson N. (1994) The system C-O in equilibrium with graphite at high pressure and temperature, An experimental study. *Geochim. Cosmochim. Acta* **58**, 9-17.
- Jarosewich E., Nelen J.A. and Norberg J.A. (1979) Electron microprobe reference samples for mineral analyses. *Smithsonian Contrib. to Earth Sci.* **20**, 68-72.
- Jugo, P.J., Luth, R.W., Richards, J.P. (2005) An experimental study of sulfur content in basaltic melts saturated with immiscible sulfide or sulfate liquids at 1300°C and 1.0 GPa. *J. Petrol.* **46**, 783-798.

- Jugo, P.J. (2009) Sulfur content at sulfide saturation in oxidized magmas. *Geology* **37**, 415-418.
- Jego S., Dasgupta R. (2013) Fluid-present melting of sulfide-bearing ocean-crust: experimental constraints on the transport of sulfur from slab to mantle wedge. *Geochim. Cosmochim. Acta.* **110**, 106-134.
- Katsura T. & Nagashima S. (1974) Solubility of sulfur in some magmas at 1 atmosphere. *Geochim. Cosmochim. Acta* **38**, 517-531.
- King P.L., Vennemann T.W., Holloway J.R., Hervig R.L., Lowenstern J. B., Forneris J.F. (2002) Analytical techniques for volatiles: a case study using intermediate (andesitic) glasses. *Am. Mineral.* **87**, 1077-1089.
- Koptev-Dvornikov E.V., Aryaeva N.S., Bychkov D.A. (2012) Equation of thermobarometer for description of sulfide-silicate liquid immiscibility in basaltic systems. *Petrology* **20**, 450-466.
- Le Losq C., Neuville D.R., Moretti R., Roux J. (2012) Determination of water content in silicate glasses using Raman spectrometry : implications for the study of explosive volcanism. *Am. Mineral.* **97**, 779-790.
- Li C. & Ripley E.M. (2005) Empirical equations to predict the sulfur content of mafic magmas at sulfide saturation and applications to magmatic sulfide deposits. *Mineral. Deposit.* **40**, 218-230.

- Li C. & Ripley E.M. (2009) Sulfur contents at sulfide-liquid or anhydrite saturation in silicate melts: empirical equations and example applications. *Econ. Geol.* **104**, 405-412.
- Liu Y., Zhang Y.X., Behrens H. (2005) Solubility of H₂O in rhyolitic melts at low pressures and a new empirical model for mixed H₂O-CO₂ solubility in rhyolitic melts. *J. Volcan. Geotherm. Research* **143**, 219-235.
- Liu Y.N., Samaha N.T., Baker D.R. (2007) Sulfur concentration at sulfide saturation (SCSS) in magmatic silicate melts. *Geochim. Cosmochim. Acta* **71**, 1783-1799.
- Long D.A. (1977) Raman Spectroscopy, 276 p. MacGraw-Hill, New York.
- Luhr J.F. (1990) Experimental phase relations of water- and sulfur-saturated arc magmas and the 1982 eruptions of El Chichón volcano. *J. Petrol.* **31**, 1071-1114.
- Mavrogenes J.A. & O'Neill H. St.C. (1999) The relative effects of pressure, temperature and oxygen fugacity on the solubility of sulfide in mafic magmas. *Geochim. Cosmochim. Acta* **63**, 1173-1180.
- Moore G., Vennemann T., Carmichael I.S.E. (1998) An empirical model for the solubility of H₂O in magmas to 3 kilobars. *Am. Mineral.* **83**, 36-42.
- Moune S., Holtz F., Botcharnikov R.E. (2009) Sulphur solubility in andesitic to basaltic melts: implications for Hekla volcano. *Contrib. Mineral. Petrol.* **157**, 691-707.

- Moretti R., Papale P., Ottonello G. (2003) A model for the saturation of C-H-O-S fluids in silicate melts. In *Volcanic Degassing* (eds. C. Oppenheimer, D.M. Pyle, J. Barclay). Geol. Soc. London Special Pub. **213**, pp. 81-101.
- Moretti R. & Ottonello G. (2003) Polymerization and disproportionation of iron and sulfur in silicate melts: insights from an optical basicity-based approach. *J. Non-Cryst. Solids* **323**, 111-119.
- Moretti R. & Ottonello G. (2005) Solubility and speciation of sulfur in silicate melts, the conjugated Toop-Samis-Grjotheim (CTSFG) model. *Geochim. Cosmochim. Acta* **69**, 801-823.
- Mueller-Simon H. (2011) Fining of glass melts. In *Sulfur in Magmas and Melts and its Importance for Natural and Technical Processes* (eds. H. Behrens and J.D. Webster). Mineral Society of America, Reviews in Mineralogy **73**, pp. 337-361.
- Mysen B.O. & Richet P. (2005) *Developments in Geochemistry 10, Silicate glasses and melts properties and structure*. Elsevier, Amsterdam.
- O'Neill H. St.C. & Mavrogenes J.A. (2002) The sulfide capacity and the sulfur content at sulfide saturation of silicate melts at 1400 °C and 1 bar. *J. Petrol.* **43**, 1049-1087.
- Oppenheimer C., Scailler B., Martin R.S. (2011) Sulfur degassing from volcanoes: source conditions, surveillance, plume chemistry and earth system impacts. In *Sulfur in Magmas and Melts and its Importance for Natural and Technical*

- Processes* (eds. H. Behrens and J.D. Webster). Mineral Society of America, Reviews in Mineralogy **73**, pp. 363-421.
- Peach C.L., Mathez E.A. (1993) Sulfide melt-silicate melt distribution coefficients for nickel and iron and implications for the distribution of other chalcophile elements. *Chemochim Cosmochim Acta* **57**, 3013-3021.
- Peach C.L., Mathez E.A., Keays R.R., Reeves S.J. (1994) Experimentally determined sulfide melt-silicate partition coefficients for iridium and palladium. *Chem. Geol.* **117**, 361-377.
- Poulson S.R. & Ohmoto H. (1990) An evaluation of the solubility of sulfide sulfur in silicate melts from experimental data and natural samples. *Chem. Geol.* **85**, 57-75.
- Richardson F.D., Fincham C.J.B. (1954) Sulphur in silicate and aluminate slags. *J. Iron Steel Inst.* **178** 4-15.
- Righter K., Pando K., Danielson L.R., (2009) Experimental evidence for the sulfur-rich martian magmas: implications for volcanism and surficial sulfur sources. *Earth Planet. Sci. Lett.* **288**, 235-243.
- Rosenqvist T. (1951) A thermodynamic study of the reaction $\text{CaS} + \text{H}_2\text{O} = \text{CaO} + \text{H}_2\text{S}$ and the desulphurization of liquid metals with lime. *Trans. Am. Inst. Mining Metall. Eng.* **191**, 535-540.

- Rutherford M.J. & Devine J.D. (1996) Preeruption pressure-temperature conditions and volatiles in the 1991 dacitic magma of Mount Pinatubo. In *Fire and Mud: Eruptions and Lahars of Mount Pinatubo, Philippines* (eds. C.G. Newhall CG and R.S. Punongbayan) Univ. Washington Press, Seattle, pp. 751-766.
- Ryerson F.J. & Watson E.B. (1987) Rutile saturation in magmas, implications for Ti-Nb-Ta depletion in island-arc basalts. *Earth Planet. Sci. Lett.* **86**, 225-239.
- Sattari P., Brenan J.M., Horn I., McDonough W.F. (2002) Experimental constraints on the sulfide- and chromite-silicate melt partitioning behavior of rhenium and platinum-group elements. *Econ. Geol.* **91**, 385-398.
- Scaillet B. & Pichavant M. (2005) A model of sulphur solubility for hydrous mafic melts: application to the determination of magmatic fluid compositions of Italian volcanoes. *Annal. Geophys.* **48**, 671-698.
- Shima J. & Naldrett A.J. (1975) Solubility of sulfur in an ultramafic melt and the relevance of the system Fe-S-O. *Econ. Geol.* **70**, 960-967.
- Simon A.C., & Ripley, E.M. (2011) The role of magmatic sulfur in the formation of ore deposits. In *Sulfur in Magmas and Melts and its Importance for Natural and Technical Processes* (eds. H. Behrens and J.D. Webster). Mineral Society of America, Reviews in Mineralogy **73**, pp. 513-578.

- Sobolev A.V., Chaussidon M. (1996) H₂O concentrations in primary melts from supra-subduction zones and mid-ocean ridges: implications for H₂O storage and recycling in the mantle. *Earth Planet. Sci. Lett.*, **137**, 45-55.
- Stern R.J. (1979) Origin of andesite in the Northern Mariana island arc – implications from Agrigan. *Contrib. Mineral. Petrol.* **68**, 207-219.
- Stolper, E. (1982) The speciation of water in silicate melts. *Geochim. Cosmochim. Acta* **46**, 2609-2620.
- Symonds R.B., Rose W.I., Bluth G.S. and Gerlach T.M. (1994) Volcanic gas studies, methods, results and applications. In *Volatiles in Magmas* (eds. M.R. Carroll and J.R. Holloway). Mineral Society of America, Reviews in Mineralogy **30**, pp. 1-66.
- Thomas R. (2000) Determination of water concentrations of granite melt inclusion by confocal laser Raman microprobe spectroscopy. *Am Mineral.* **85**, 868-872.
- Tsujimura T., Kitakaze A. (2005) Experimental study of sulfur solubility in silicate melts coexisting with graphite as a function of silicate melt composition. *Res. Geol.* **55**, 55-60.
- Wallace P. & Carmichael I.S.E. (1992) Sulfur in basaltic magmas. *Geochim. Cosmochim. Acta* **56**, 1863-1874.

Wilke M., Jugo P.J., Klimm, K., Susini, J., Botcharnikov R., Kohn S.C., Janousch M.

(2008) The origin of S⁴⁺ detected in silicate glasses by XANES. *Am. Mineral.* **93**, 235-240.

Wilke M., Klimm K., Kohn S.C. (2011) Spectroscopic studies on sulfur speciation in synthetic and natural glasses. In *Sulfur in Magmas and Melts and its Importance for Natural and Technical Processes* (eds. H. Behrens and J.D. Webster). Mineral Society of America, Reviews in Mineralogy **73**, pp. 41-78.

Wendlandt R.F. (1982) Sulfide saturation of basalt and andesite melts at high pressures and temperatures. *Am. Mineral.* **67**, 877-885.

Zajacz Z., Candela P.A., Piccoli P.M., Sanchez-Valle C., Walle M. (2013) Solubility and partitioning behavior of Au, Cu, Ag and reduced S in magmas. *Geochim. Cosmochim. Acta* **112**, 288-304.

APPENDIX I: Calibration Dataset

T(K)	P (GPa)	log fO ₂	SiO ₂	TiO ₂	Al ₂ O ₃	FeO*	MnO	MgO	CaO	Na ₂ O	K ₂ O	H ₂ O		run#	Source	water method	
												P ₂ O ₅	wt. %				
1523	1	-8.87	58.0	0.79	15.26	7.72	0.22	1.88	5.43	3.52	1.73	0.36	7.3	1265	MAF-45	1	Raman
1523	1	-8.87	58.3	0.82	15.39	7.66	0.20	1.88	5.42	3.65	1.87	0.37	4.6	1167	MAF-38	1	Raman
1523	1	-8.87	58.5	0.78	15.42	7.65	0.23	1.90	5.41	3.74	1.92	0.38	4.1	1094	MAF-36	1	Raman
1523	1	-8.87	58.9	0.80	15.62	7.86	0.23	1.92	5.54	3.97	1.97	0.38	4.4	776	MAF-32	1	Raman
1523	1	-8.87	59.1	0.80	15.91	8.51	0.25	1.97	5.67	4.06	1.97	0.39	0.0	707	MAF-28	1	Raman
1523	1	-8.87	59.0	0.79	15.64	7.83	0.23	1.93	5.54	3.91	1.94	0.38	2.1	615	MAF-34	1	Raman
1523	1	-8.87	72.6	0.10	12.32	0.97	0.00	0.00	0.97	0.08	0.06	0.00	4.2	595	MAF-44	1	Raman
1523	1	-8.87	73.9	0.10	12.56	0.81	0.00	0.00	0.81	0.08	0.07	0.00	3.4	480	MAF-39	1	Raman
1523	1	-8.87	75.3	0.11	12.87	0.67	0.00	0.00	0.67	0.07	0.06	0.00	0.0	222	MAF-31	1	Raman
1523	1	-8.87	75.0	0.11	12.80	0.85	0.00	0.00	0.85	0.07	0.07	0.00	0.0	181	MAF-33	1	Raman
1523	1	-8.87	75.7	0.12	12.94	0.67	0.00	0.00	0.67	0.09	0.06	0.00	0.0	181	MAF-27	1	Raman
1523	1	-8.87	75.7	0.12	13.00	0.59	0.00	0.00	0.59	0.07	0.07	0.00	0.0	143	MAF-35	1	Raman
1523	1	-8.87	49.6	1.33	14.90	8.08	0.15	8.59	11.29	2.25	0.09	0.09	5.9	1765	MAF-12	1	Raman
1523	1	-8.87	48.9	1.31	14.70	9.59	0.15	8.79	11.28	2.32	0.09	0.10	2.8	1409	MAF-15	1	Raman
1523	1	-8.87	50.2	1.26	15.40	9.03	0.17	9.05	11.50	2.39	0.10	0.10	2.6	1248	MAF-9	1	Raman
1523	1	-8.87	49.8	1.31	15.80	10.10	0.17	8.58	11.24	2.48	0.09	0.11	0.7	1246	MAF-7	1	Raman
1523	1	-8.87	49.7	1.41	16.10	10.30	0.17	7.85	10.85	2.65	0.10	0.11	0.0	1218	MAF-19	1	Raman
1523	1	-8.87	49.9	1.38	16.60	10.50	0.16	7.77	10.79	2.71	0.12	0.12	0.9	1180	MAF-4	1	Raman
1723	1	-7.34	48.4	2.65	16.00	7.57	0.17	6.06	11.19	2.45	1.01	0.68	0.0	2800	GS-13	2	anhydrous
1723	1	-7.34	49.9	2.72	16.51	6.42	0.12	6.65	11.70	3.21	0.95	0.73	0.0	2060	GS-17	2	anhydrous
1673	1	-7.68	51.6	2.87	17.00	1.42	0.15	6.85	12.58	3.43	1.04	0.73	0.0	1770	GS-2	2	anhydrous
1573	1	-8.43	49.9	2.72	16.32	6.91	0.11	6.75	11.84	3.12	0.90	0.70	0.0	1490	GS-15	2	anhydrous
1573	1	-8.43	49.4	2.75	16.13	5.87	0.13	6.65	11.59	2.99	0.95	0.68	0.0	1460	GS-18	2	anhydrous
1673	1	-7.68	52.6	2.80	17.35	0.10	0.04	6.79	12.86	3.25	0.95	0.75	0.0	1240	GS-3	2	anhydrous
1498	1	-9.09	48.8	4.04	17.14	5.39	0.16	6.25	10.34	3.57	1.60	1.24	0.0	525	STE-7	2	anhydrous

1473	0.2	-7.80	45.9	1.58	14.53	10.01	0.30	9.61	9.34	3.04	1.72	0.49	1.7	3000	S8	3	IR
1473	0.2	-6.80	47.0	1.63	14.96	9.02	0.17	9.85	9.67	3.07	1.77	0.55	1.7	2200	S2	3	IR
1323	0.193	-9.70	46.7	1.67	16.05	7.72	0.17	5.56	10.31	3.50	1.84	0.51	5.9	1200	0_15_2 red	3	IR
1473	0.0001	-7.40	40.0	4.84	8.02	23.42	0.15	7.61	10.93	1.78	0.94	0.67	0.0	5136	cent 100	4	anhydrous
1473	0.0001	-8.83	40.7	4.92	8.19	21.97	0.11	8.01	11.09	1.58	0.89	0.77	0.0	4605	cent 92	4	anhydrous
1473	0.0001	-9.25	42.6	5.31	8.58	18.61	0.11	7.61	11.89	1.49	0.77	0.83	0.0	3798	cent 91	4	anhydrous
1473	0.0002	-7.83	44.7	5.09	8.48	17.84	0.09	8.94	11.34	1.49	0.77	0.51	0.0	3349	cent 108	4	anhydrous
1573	0.9	-8.56	46.6	1.49	12.63	21.13	0.21	7.06	8.33	2.42	0.00	0.00	0.0	3089	lr1e	4	anhydrous
1473	0.0001	-9.51	45.6	5.26	8.56	15.85	0.12	8.93	11.72	1.46	0.68	0.86	0.0	2932	cent 81	4	anhydrous
1473	0.9	-9.49	46.4	1.77	13.72	21.32	0.19	5.05	8.44	2.88	0.00	0.00	0.0	2820	Hpsulf 7e	4	anhydrous
1473	0.0001	-9.65	46.5	5.39	8.57	13.79	0.15	8.74	11.91	1.63	1.01	0.71	0.0	2716	cent 98	4	anhydrous
1473	0.0001	-8.45	48.4	5.56	8.75	11.78	0.12	9.19	11.96	1.59	0.93	0.87	0.0	2267	cent 83	4	anhydrous
1473	0.0001	-8.46	47.5	5.56	8.89	11.27	0.12	9.51	12.09	1.78	1.07	0.83	0.0	2104	cent 87	4	anhydrous
1473	0.0001	-8.50	50.7	1.79	14.93	11.94	0.16	9.06	9.45	1.87	0.00	0.00	0.0	1947	fO2#4e	4	anhydrous
1523	1.5	-8.20	47.7	1.59	13.48	18.96	2.61	5.69	8.12	0.13	0.00	0.00	0.0	1916	Hpsulf 26e	4	anhydrous
1473	1.5	-8.53	48.6	1.68	14.22	17.56	0.13	4.75	7.89	1.98	0.00	0.00	0.0	1797	Hpsulf 27e	4	anhydrous
1473	0.0002	-8.37	49.6	5.69	8.74	9.97	0.15	9.73	11.99	1.79	1.06	0.63	0.0	1778	cent 109	4	anhydrous
1473	0.0001	-8.89	50.4	5.59	9.34	8.18	0.07	9.82	12.03	1.49	0.99	0.92	0.0	1615	cent 95	4	anhydrous
1473	0.0001	-7.72	51.7	6.09	9.57	5.89	0.09	9.76	12.15	1.79	1.13	0.98	0.0	1284	cent 85	4	anhydrous
1473	0.0001	-7.83	50.9	6.33	10.39	4.76	0.07	11.02	12.77	1.09	0.58	0.99	0.0	1256	cent 89	4	anhydrous
1523	1.5	-8.20	50.8	1.79	14.67	10.75	0.12	6.19	8.83	2.66	0.00	0.00	0.0	912	Hpsulf 30	4	anhydrous
1473	1.5	-8.53	51.5	1.92	15.46	11.71	0.14	4.57	7.99	2.98	0.00	0.00	0.0	768	Hpsulf 19	4	anhydrous
1473	1.5	-8.53	54.6	1.91	15.24	3.91	0.12	6.35	8.49	1.88	0.00	0.00	0.0	726	Hpsulf 46	4	anhydrous
1873	1	-6.40	48.5	0.36	6.10	14.30	0.40	20.90	6.90	0.54	0.04	0.15	1.1	5540	B152	5	FTIR
1873	1	-6.40	46.5	0.65	10.00	16.40	0.44	9.23	12.90	1.78	0.17	0.55	0.1	5000	B163	5	FTIR
1873	1	-6.40	50.9	0.40	6.02	15.00	0.39	18.40	6.96	0.47	0.05	0.16	0.0	4800	B159	5	anhydrous
1973	2	-4.99	46.7	0.53	10.77	17.30	0.44	9.58	13.55	1.62	0.16	0.59	0.0	4800	B188	5	anhydrous
1873	1.5	-5.95	45.6	0.50	10.90	17.00	0.43	9.30	13.00	1.65	0.15	0.56	0.0	4800	B167	5	anhydrous
1873	1	-6.40	49.0	0.63	8.30	15.70	0.08	9.92	13.35	1.87	0.15	0.46	1.7	4700	B197	5	FTIR

1873	1	-6.40	47.5	0.63	9.90	12.10	0.40	11.00	15.60	1.78	0.18	0.48	0.0	4700	B181	5	anhydrous
1923	2	-5.23	46.0	0.63	10.70	17.70	0.44	9.50	13.40	1.70	0.17	0.58	0.0	4600	B186	5	anhydrous
1873	2	-5.49	45.3	0.51	10.59	16.40	0.42	9.60	13.50	1.69	0.16	0.56	0.0	4200	B165	5	anhydrous
1873	1.5	-5.95	49.5	0.38	6.20	13.40	0.38	20.60	7.50	0.45	0.03	0.17	0.0	4100	B160	5	anhydrous
1873	2	-5.49	49.8	0.52	5.80	17.00	0.49	19.60	6.60	0.53	0.03	0.17	0.0	3800	B161	5	anhydrous
1873	2.5	-7.34	45.9	0.49	10.60	15.80	0.40	9.90	13.89	1.64	0.16	0.59	0.0	3700	B164	5	anhydrous
1823	2	-5.76	47.3	0.60	9.68	17.40	0.43	9.07	13.04	1.71	0.16	0.52	0.0	3600	B190	5	anhydrous
1873	2.5	-7.34	48.9	0.47	7.10	17.10	0.51	17.20	7.63	0.60	0.05	0.19	0.0	3500	B162	5	anhydrous
1873	4	-3.66	46.6	0.60	9.55	13.90	0.46	11.50	13.70	1.43	0.14	0.52	0.0	3400	MA38	5	anhydrous
1923	5	-2.57	44.8	0.48	10.30	13.50	0.45	12.40	14.60	1.40	0.13	0.58	0.0	3400	MA36	5	anhydrous
1773	2	-6.04	45.8	0.55	11.30	16.50	0.46	9.90	13.71	1.67	0.16	0.62	0.0	3300	B189	5	anhydrous
1873	3	-4.58	45.6	0.47	11.40	15.70	0.47	10.70	14.79	1.63	0.16	0.63	0.0	3000	B191	5	anhydrous
1873	5	-2.75	45.6	0.55	11.30	14.40	0.46	11.50	14.10	1.44	0.18	0.61	0.0	2800	MA37	5	anhydrous
1473	0.0001	-9.64	41.8	1.51	15.65	26.24	0.00	3.68	7.24	1.66	1.23	0.00	0.0	2690	8F1	6	anhydrous
1473	0.0001	-8.86	43.8	1.61	17.13	22.19	0.00	3.94	7.31	2.55	1.12	0.00	0.0	2320	9F2	6	anhydrous
1473	0.0001	-8.95	44.8	1.66	17.79	18.97	0.00	4.40	7.80	2.32	1.15	0.00	0.0	2190	10F2	6	anhydrous
1473	0.0001	-10.35	38.9	1.57	22.46	17.92	0.00	5.11	8.50	2.93	1.12	0.00	0.0	1950	14F2	6	anhydrous
1473	0.0001	-9.41	44.0	1.69	19.26	18.69	0.00	4.58	7.50	2.40	1.20	0.00	0.0	1880	7F1	6	anhydrous
1473	0.0001	-9.40	46.3	1.86	18.54	15.43	0.00	3.96	6.96	3.83	1.55	0.00	0.0	1790	13F1	6	anhydrous
1473	0.0001	-11.08	47.5	1.80	17.16	15.19	0.00	5.71	8.47	2.91	1.61	0.00	0.0	1620	13F1	6	anhydrous
1473	0.0001	-9.31	45.1	1.78	19.81	16.41	0.00	5.74	7.31	2.64	0.94	0.00	0.0	1580	11F2	6	anhydrous
1473	0.0001	-9.31	44.1	1.70	20.96	15.81	0.00	5.11	6.94	3.54	1.32	0.00	0.0	1350	9F1	6	anhydrous
1473	0.0001	-9.01	46.0	1.93	22.89	13.83	0.00	5.19	6.85	2.35	0.85	0.00	0.0	1260	2F2	6	anhydrous
1473	0.0001	-9.17	49.2	0.00	19.68	12.45	0.00	5.83	8.08	2.24	0.81	0.00	0.0	1070	2F1	6	anhydrous
1473	0.0001	-9.08	48.0	1.95	17.09	14.17	0.00	6.39	7.25	2.61	1.21	0.00	0.0	1040	6F1	6	anhydrous
1473	0.0001	-9.30	52.0	2.06	16.22	10.55	0.00	6.63	8.11	2.40	1.25	0.00	0.0	810	31F1	6	anhydrous
1473	0.0001	-8.90	49.2	1.93	19.18	12.80	0.00	6.04	7.82	2.56	0.88	0.00	0.0	800	1F2	6	anhydrous
1473	0.0001	-9.46	49.2	1.97	20.53	11.82	0.00	5.70	7.86	2.08	1.08	0.00	0.0	770	3F1	6	anhydrous
1473	0.0001	-9.73	52.5	2.12	16.20	9.74	0.00	6.04	8.54	2.46	1.13	0.00	0.0	710	4F1	6	anhydrous

1473	0.0001	-10.20	53.9	2.12	20.06	6.51	0.00	6.24	8.73	1.81	0.88	0.00	0.0	480	1F1	6	anhydrous
1473	0.0001	-11.08	53.1	2.52	20.93	5.28	0.00	8.27	6.27	2.81	1.58	0.00	0.0	450	12F1	6	anhydrous
1473	0.0001	-11.08	54.7	2.21	20.31	3.11	0.00	7.80	7.66	3.50	4.64	0.00	0.0	430	11F1	6	anhydrous
1773	0.9	-9.52	51.0	0.37	10.10	17.20	0.29	10.50	8.99	0.16	0.04	0.00	0.0	3320	FeS-SSKOM-14	7	anhydrous
1773	1	-9.99	50.6	0.28	9.30	10.60	0.23	19.90	8.09	0.21	0.05	0.00	0.0	3270	FeS-SSKOM-26	7	anhydrous
1873	1	-9.08	47.8	0.00	11.10	11.20	0.00	11.80	17.10	0.00	0.00	0.00	0.0	2960	FeS-BK-4	7	anhydrous
1773	1	-9.89	50.0	0.25	8.55	12.80	0.25	20.70	7.09	0.19	0.04	0.00	0.0	2910	FeS-SSKOM-25	7	anhydrous
1873	1	-8.98	42.2	0.00	13.40	12.60	0.00	22.10	8.72	0.00	0.00	0.00	0.0	2870	FeS-BK-13	7	anhydrous
1798	1	-9.88	46.4	0.00	10.10	9.27	0.00	19.70	14.00	0.00	0.00	0.00	0.0	2660	FeS-BK-8	7	anhydrous
1773	1.4	-9.67	49.2	0.29	9.77	14.00	0.26	17.80	8.16	0.09	0.04	0.00	0.0	2390	FeS-SSKOM-15	7	anhydrous
1723	1	-10.33	50.4	0.27	8.36	12.30	0.25	19.80	7.97	0.00	0.03	0.00	0.0	2300	FeS-SSKOM-12	7	anhydrous
1723	1	-10.33	50.8	0.27	8.77	12.80	0.25	17.90	8.51	0.06	0.03	0.00	0.0	2230	FeS-SSKOM-11	7	anhydrous
1723	1	-10.73	46.3	0.00	12.00	7.06	0.00	17.20	16.50	0.00	0.00	0.00	0.0	2170	FeS-AD-1	7	anhydrous
1773	2	-9.48	47.0	0.56	14.20	12.50	0.25	9.65	13.90	0.31	0.10	0.00	0.0	2150	FeS-SSKOM-16	7	anhydrous
1723	1	-10.63	50.8	2.12	7.79	8.37	0.11	14.50	4.16	0.73	8.39	0.00	0.0	2130	FeS-I-10-08-1	7	anhydrous
1773	2.5	-9.73	50.8	0.13	6.95	8.93	0.25	22.20	10.00	0.05	0.00	0.00	0.0	2060	FeS-SSKOM-17	7	anhydrous
1723	1	-10.53	47.0	0.00	10.60	8.63	0.00	16.40	16.70	0.00	0.00	0.00	0.0	2050	FeS-BK-9	7	anhydrous
1723	1	-10.53	50.8	0.33	10.50	9.23	0.20	18.40	10.20	0.23	0.05	0.00	0.0	2030	FeS-SSKOM-6	7	anhydrous
1723	1	-10.53	50.3	0.36	11.10	9.86	0.22	16.80	10.40	0.27	0.05	0.00	0.0	1990	FeS-SSKOM-7	7	anhydrous
1773	2	-9.68	47.1	0.50	14.50	9.87	0.23	12.60	13.30	0.24	0.08	0.00	0.0	1940	FeS-SSKOM-27	7	anhydrous
1723	1	-10.63	49.7	0.40	12.10	8.76	0.22	16.50	11.80	0.29	0.05	0.00	0.0	1910	FeS-SSKOM-5	7	anhydrous
1723	1.6	-10.14	46.0	0.62	14.90	13.50	0.33	11.50	12.00	0.03	0.17	0.00	0.0	1850	FeS-SSKOM-2	7	anhydrous
1673	1	-10.70	44.8	0.00	17.80	11.90	0.00	6.25	17.60	0.00	0.00	0.00	0.0	1810	FeS-BK12	7	anhydrous
1698	1.5	-10.40	46.0	1.01	16.20	13.50	0.34	8.52	13.10	0.66	0.30	0.00	0.0	1780	FeS-SSKOM-1	7	anhydrous
1773	2.7	-9.96	47.7	0.21	14.60	6.11	0.31	22.40	8.47	0.14	0.00	0.00	0.0	1740	FeS-SSKOM-24	7	anhydrous
1723	1	-10.73	53.0	0.34	10.80	7.78	0.22	17.90	10.10	0.04	0.04	0.00	0.0	1730	FeS-SSKOM-13	7	anhydrous
1773	2.4	-10.16	50.0	0.21	9.66	5.92	0.26	22.60	10.80	0.24	0.00	0.00	0.0	1610	R-FeS-SSKOM-23	7	anhydrous
1723	1	-10.63	51.7	0.56	13.50	7.93	0.15	13.80	8.15	3.17	0.77	0.00	0.0	1500	FeS-85-41c-1	7	anhydrous
1643	1.4	-11.46	50.5	0.08	20.20	7.89	0.13	6.90	10.10	4.46	0.16	0.00	0.0	1260	FSOs-15-7	7	anhydrous

1643	1.4	-11.56	50.1	1.07	19.90	7.02	0.11	5.22	7.48	6.38	0.84	0.00	0.0	750	FSOs-15-6	7	anhydrous
1628	1.6	-7.39	47.6	0.69	17.90	7.80	0.00	12.60	11.00	2.20	0.00	0.00	0.0	1600	11	8	anhydrous
1573	1	-8.85	47.1	0.70	17.70	8.70	0.00	11.90	10.80	2.21	0.00	0.00	0.0	1600	52B	8	anhydrous
1588	1.2	-8.11	48.0	0.61	18.40	5.10	0.00	12.60	11.50	1.78	0.00	0.00	0.0	1500	35B	8	anhydrous
1628	1.6	-7.39	47.5	0.72	18.00	8.30	0.00	11.50	10.90	2.40	0.00	0.00	0.0	1500	7	8	anhydrous
1628	1.6	-7.39	47.9	0.74	18.30	7.90	0.00	11.50	11.40	2.40	0.00	0.00	0.0	1400	5	8	anhydrous
1628	1.6	-7.39	47.7	0.72	18.20	8.20	0.00	11.40	11.10	2.40	0.00	0.00	0.0	1400	4	8	anhydrous
1628	1.6	-7.39	47.7	0.72	18.50	8.20	0.00	10.90	11.30	2.50	0.00	0.00	0.0	1400	12	8	anhydrous
1628	1.6	-7.39	47.4	0.73	18.10	8.60	0.00	11.20	11.00	2.40	0.00	0.00	0.0	1400	2	8	anhydrous
1628	1.6	-7.39	47.9	0.68	18.20	7.00	0.00	12.10	11.40	2.30	0.00	0.00	0.0	1300	3	8	anhydrous
1573	1	-8.02	50.1	0.71	17.40	5.20	0.00	11.60	11.90	2.60	0.00	0.00	0.0	1100	54A	8	anhydrous
1573	1	-8.06	50.1	0.73	18.00	5.30	0.00	11.10	11.60	2.52	0.00	0.00	0.0	1100	54B	8	anhydrous
1588	1.1	-8.22	49.0	0.67	18.30	4.90	0.00	11.90	12.10	2.60	0.00	0.00	0.0	1100	27	8	anhydrous
1623	1	-8.05	50.4	1.24	15.40	9.14	0.17	9.12	11.22	2.49	0.00	0.12	0.0	1778	MB3	9	anhydrous
1723	1	-7.34	52.9	1.31	16.16	4.40	0.15	9.72	12.03	2.52	0.10	0.11	0.0	1770	MB5	9	anhydrous
1673	1	-7.68	50.6	1.27	15.51	8.37	0.18	9.33	11.38	2.47	0.00	0.10	0.0	1752	MB4	9	anhydrous
1523	1	-8.87	50.0	1.28	16.05	9.90	0.19	8.48	11.02	2.59	0.00	0.12	0.0	1214	MB1	9	anhydrous
1703	1	-7.47	58.5	0.82	15.95	8.24	0.23	1.96	5.58	4.07	1.96	0.37	0.0	1070	yn40	9	anhydrous
1623	1	-8.06	59.9	0.75	16.24	8.42	0.21	2.02	5.30	4.17	1.96	0.36	0.0	1055	yn28	9	anhydrous
1673	1	-7.68	60.5	0.79	16.19	7.94	0.21	1.97	5.57	4.21	2.01	0.37	0.0	1002	yn18	9	anhydrous
1523	1	-5.71	63.2	0.54	17.35	5.20	0.00	1.79	5.10	4.27	1.80	0.00	0.0	921	yn73	9	anhydrous
1523	1	-8.87	60.0	0.78	16.11	8.24	0.23	1.98	5.43	4.13	1.95	0.36	0.0	834	yn20	9	anhydrous
1598	1	-8.25	60.2	0.80	16.02	7.83	0.22	1.92	5.59	4.19	2.02	0.36	0.0	828	yn50	9	anhydrous
1723	1	-7.34	63.6	0.52	17.76	4.68	0.00	1.77	5.45	5.84	1.75	0.00	0.0	786	TS15	9	anhydrous
1573	1	-8.45	60.0	0.83	15.86	8.06	0.23	2.02	5.63	4.06	2.00	0.38	0.0	768	yn4	9	anhydrous
1523	1	-8.87	60.3	0.76	16.01	8.01	0.22	1.95	5.58	4.13	2.00	0.37	0.0	739	yn2	9	anhydrous
1523	1	-8.87	60.1	0.80	16.01	8.30	0.24	1.98	5.69	4.08	2.01	0.37	0.0	737	yn36	9	anhydrous
1523	0.5	-9.43	59.6	0.85	15.96	8.40	0.22	1.94	5.44	3.93	2.00	0.37	0.0	726	yn12	9	anhydrous
1523	1	-8.87	59.3	0.80	15.94	8.25	0.24	1.97	5.60	4.05	2.01	0.37	0.0	700	yn35	9	anhydrous

1673	1	-7.68	63.7	0.52	17.64	4.77	0.00	1.70	5.36	4.45	1.78	0.00	0.0	697	TS13	9	anhydrous
1523	0.5	-9.43	60.6	0.80	16.30	8.23	0.25	2.00	5.73	4.00	1.99	0.38	0.0	681	yn38	9	anhydrous
1423	1	-9.79	58.2	0.80	16.00	9.14	0.24	2.10	5.94	4.03	1.89	0.39	0.0	577	yn96	9	anhydrous
1623	1	-8.06	62.1	0.52	17.83	4.59	0.00	1.70	5.34	5.91	1.80	0.00	0.0	546	TS11	9	anhydrous
1723	1	-7.34	75.7	0.10	13.06	0.79	0.00	0.07	0.57	5.27	4.73	0.00	0.0	499	TS16	9	anhydrous
1523	1	-8.87	63.4	0.52	17.68	4.59	0.00	1.79	5.46	4.43	1.75	0.00	0.0	466	TS3	9	anhydrous
1573	1	-8.45	63.2	0.54	17.82	4.95	0.00	1.77	5.44	5.17	1.78	0.00	0.0	438	TS7	9	anhydrous
1673	1	-7.68	53.1	1.05	18.86	8.77	0.20	3.43	7.90	3.98	0.97	0.24	0.0	1968	yn64	9	anhydrous
1673	1	-7.68	76.1	0.11	13.03	0.78	0.08	0.07	0.57	4.00	4.68	0.00	0.0	323	TS14	9	anhydrous
1523	1	-8.87	75.9	0.11	13.03	0.73	0.09	0.07	0.57	4.19	4.74	0.00	0.0	172	TS6	9	anhydrous
1523	1	-8.87	75.6	0.11	13.03	0.70	0.09	0.07	0.56	4.17	4.71	0.00	0.0	155	TS4	9	anhydrous
1523	1	-8.87	75.5	0.12	12.93	0.73	0.00	0.08	0.55	4.23	4.62	0.00	0.0	144	TS2	9	anhydrous
1423	1	-9.79	74.6	0.12	12.75	0.81	0.00	0.07	0.56	4.19	4.73	0.00	0.0	96	yn92	9	anhydrous
1423	1	-9.79	74.6	0.11	12.89	0.83	0.07	0.07	0.53	4.19	4.74	0.00	0.0	80	yn94	9	anhydrous
1773	0.5	-8.65	47.7	1.77	10.74	12.20	0.00	16.87	8.51	1.79	0.34	0.00	0.0	4010	MAV34	10	anhydrous
2073	1	-6.29	47.1	0.90	9.92	15.49	0.00	15.18	8.83	1.89	0.37	0.00	0.0	3370	MAV58A	10	anhydrous
1773	1.5	-8.34	47.3	1.78	9.48	15.56	0.00	15.68	8.45	1.50	0.33	0.00	0.0	3125	MAV36	10	anhydrous
2073	0.5	-6.42	50.2	1.72	17.07	10.71	0.00	7.25	9.33	2.64	0.80	0.00	0.0	2955	MAV54	10	anhydrous
1773	1.5	-8.34	48.6	1.64	10.47	11.47	0.00	17.01	8.35	1.51	0.34	0.00	0.0	2750	MAV42	10	anhydrous
2073	3.5	-5.63	50.9	1.65	17.23	9.31	0.00	7.58	10.15	2.09	0.56	0.00	0.0	1875	MAV68	10	anhydrous
2073	4	-5.50	50.6	1.71	17.04	10.88	0.00	7.56	9.16	2.92	0.75	0.00	0.0	1855	MAV55	10	anhydrous
1773	0.5	-8.65	50.8	1.81	16.50	8.68	0.00	6.84	8.86	2.10	0.68	0.00	0.0	1800	MAV32	10	anhydrous
1673	0.5	-9.56	50.4	1.80	16.92	9.95	0.00	7.06	9.66	2.45	0.79	0.00	0.0	1725	MAV27	10	anhydrous
2073	4	-5.50	48.9	0.71	10.54	11.57	0.00	16.31	9.76	1.71	0.39	0.00	0.0	1650	MAV52	10	anhydrous
1673	0.5	-9.56	52.0	2.13	17.68	8.40	0.00	7.30	10.18	1.34	0.97	0.00	0.0	1640	MAV65	10	anhydrous
1773	1.5	-8.34	51.3	1.57	17.62	9.80	0.00	7.44	9.29	2.93	0.80	0.00	0.0	1570	MAV29	10	anhydrous
1673	1.5	-9.23	47.6	1.76	17.88	10.17	0.00	6.73	9.52	2.71	0.85	0.00	0.0	1380	MAV26	10	anhydrous
1673	1.5	-9.23	51.8	2.50	17.70	8.60	0.00	7.30	9.94	1.22	0.90	0.00	0.0	1220	MAV64	10	anhydrous
1773	2.5	-8.03	49.6	0.67	17.21	8.16	0.00	7.76	10.55	2.64	0.72	0.00	0.0	880	MAV31	10	anhydrous

2073	9	-4.17	49.4	1.66	16.60	6.27	0.00	10.39	10.68	2.23	0.60	0.00	0.0	615	MAV45	10	anhydrous
1323	0.312	-9.86	43.9	4.69	12.77	14.29	0.19	5.57	9.47	2.59	0.57	0.59	6.1	2590	B-12	11	KFT
1323	0.289	-10.08	44.6	4.54	12.84	13.11	0.23	5.47	9.48	2.58	0.57	0.64	5.9	2290	B-4	11	KFT
1323	0.299	-8.87	48.8	3.25	15.57	12.03	0.22	4.66	8.55	3.26	0.69	0.67	2.5	1620	B-24	11	corrected KFT
1323	0.299	-9.67	50.1	2.06	13.42	10.11	0.29	2.79	6.68	3.71	1.17	1.11	6.4	1610	HK-4	11	KFT
1323	0.299	-9.67	52.4	2.06	14.05	9.40	0.29	2.90	6.53	3.76	1.12	1.11	5.8	1500	HK-5	11	KFT
1323	0.299	-9.17	49.3	3.20	15.48	12.19	0.22	4.51	8.58	3.59	0.74	0.69	2.0	1490	B-23	11	corrected KFT
1323	0.299	-10.07	47.5	3.72	14.71	12.71	0.27	4.39	8.97	2.99	0.66	0.65	2.8	1460	B-17	11	corrected KFT
1323	0.204	-9.74	52.2	2.08	14.06	10.74	0.29	3.05	6.59	3.67	1.18	1.03	5.2	1300	HK-38	11	KFT
1323	0.299	-10.07	47.8	3.71	14.94	11.46	0.24	4.52	8.90	3.26	0.66	0.67	2.6	1260	B-18	11	corrected KFT
1323	0.204	-9.74	52.8	2.18	14.32	9.86	0.34	3.12	6.83	3.75	1.22	1.09	4.3	1100	HK-39	11	KFT
1323	0.304	-10.36	53.5	2.16	14.50	9.96	0.31	3.11	6.88	3.88	1.23	1.15	3.3	870	HK-13	11	KFT
1323	0.297	-9.67	53.6	2.18	14.40	9.93	0.31	3.15	6.96	4.04	1.21	1.05	3.3	860	HK-33	11	KFT
1323	0.304	-10.26	53.5	2.19	14.40	9.11	0.31	3.10	6.94	3.80	1.23	1.16	3.6	840	HK-14	11	KFT
1323	0.297	-9.57	53.9	2.16	14.51	9.30	0.26	3.16	6.91	3.73	1.22	1.07	3.5	790	HK-34	11	KFT
1323	0.312	-9.86	44.2	4.67	12.94	12.97	0.25	5.43	9.37	2.61	0.59	0.59	6.1	2390	B-11	11	KFT
1723	0.8	-7.53	48.2	0.83	16.14	9.18	0.11	10.45	11.98	2.07	0.10	0.00	0.0	1789	Ni25	12	anhydrous
1723	0.8	-7.53	52.1	0.82	18.27	2.82	0.09	12.11	12.68	2.14	0.08	0.00	0.0	1642	Ni2	12	anhydrous
1723	0.8	-7.53	54.2	1.55	18.26	2.86	0.00	9.05	10.10	2.72	0.64	0.00	0.0	1622	Ni27	12	anhydrous
1723	0.8	-7.53	49.0	1.24	17.49	13.47	0.00	7.84	8.39	1.85	0.44	0.00	0.0	1606	Ni16	12	anhydrous
1723	0.8	-7.53	49.5	0.77	17.04	8.18	0.14	11.39	11.98	2.12	0.13	0.00	0.0	1601	Ni1	12	anhydrous
1723	0.8	-7.53	55.9	1.63	18.69	0.98	0.00	9.98	10.61	1.87	0.53	0.00	0.0	1466	Ni13	12	anhydrous
1723	0.8	-7.53	48.8	0.77	17.02	6.93	0.16	10.40	11.82	2.45	0.10	0.00	0.0	1310	Ni6	12	anhydrous
1723	0.8	-7.53	50.9	0.86	17.75	5.07	0.18	11.26	12.13	2.27	0.13	0.00	0.0	1300	Ni5	12	anhydrous
1723	0.8	-7.53	56.2	1.62	19.22	2.37	0.00	9.04	10.10	1.98	0.53	0.00	0.0	1180	Ni20	12	anhydrous
1723	0.8	-7.53	53.2	1.36	17.76	8.25	0.00	8.73	9.30	1.78	0.45	0.00	0.0	1049	Ni19	12	anhydrous
1723	0.8	-7.53	48.5	0.73	16.43	8.84	0.16	10.42	11.85	2.23	0.11	0.00	0.0	2390	Ir11	13	anhydrous
1723	0.8	-7.53	48.2	1.42	15.85	13.85	0.00	8.19	8.72	2.29	0.51	0.00	0.0	2390	Pd13	13	anhydrous
1723	0.8	-7.53	48.6	1.45	15.92	14.03	0.00	8.11	8.63	2.14	0.52	0.00	0.0	2280	Ir19	13	anhydrous

1723	0.8	-7.53	48.3	1.46	16.01	13.83	0.00	8.20	8.69	2.07	0.47	0.00	0.0	2070	Ir20	13	anhydrous
1723	0.8	-7.53	47.9	1.48	15.95	13.58	0.00	8.34	8.96	2.32	0.47	0.00	0.0	1950	Pd14	13	anhydrous
1723	0.8	-7.53	48.5	0.74	16.46	8.62	0.16	10.49	12.02	2.15	0.09	0.00	0.0	1860	Ir7	13	anhydrous
1723	0.8	-7.53	51.0	1.53	16.97	9.23	0.01	8.65	9.21	2.23	0.48	0.00	0.0	1790	Ir17	13	anhydrous
1723	0.8	-7.53	48.7	0.75	15.94	7.90	0.16	10.97	11.92	2.48	0.08	0.00	0.0	1770	CP52	13	anhydrous
1723	0.8	-7.53	47.9	0.71	16.22	8.12	0.17	10.32	11.85	2.50	0.08	0.00	0.0	1690	CP53	13	anhydrous
1723	0.8	-7.53	49.1	0.67	18.44	8.19	0.15	10.09	11.65	2.61	0.09	0.00	0.0	1590	CP54	13	anhydrous
1723	0.8	-7.53	52.4	1.52	17.20	8.32	0.00	8.71	9.23	2.22	0.48	0.00	0.0	1550	Ir21	13	anhydrous
1723	0.8	-7.53	55.7	1.69	17.63	2.50	0.01	9.26	10.02	2.50	0.55	0.00	0.0	1540	Pd8	13	anhydrous
1723	0.8	-7.53	54.2	1.62	17.20	2.48	0.00	8.88	9.94	2.65	0.63	0.00	0.0	1490	Ir13	13	anhydrous
1723	0.8	-7.53	52.0	1.28	17.64	8.06	0.01	7.88	9.00	2.16	0.51	0.00	0.0	1490	1r24	13	anhydrous
1723	0.8	-7.53	54.8	1.49	17.42	2.58	0.00	8.95	9.79	2.63	0.67	0.00	0.0	1450	Ir12	13	anhydrous
1723	0.8	-7.53	54.4	1.62	17.55	4.60	0.01	9.09	9.86	2.56	0.52	0.00	0.0	1410	Pd10	13	anhydrous
1723	0.8	-7.53	51.1	1.54	17.15	8.77	0.01	8.67	9.34	2.49	0.51	0.00	0.0	1290	Pd11	13	anhydrous
1723	0.8	-7.53	51.1	1.52	17.12	8.86	0.00	8.58	9.21	2.41	0.53	0.00	0.0	1280	Ir18	13	anhydrous
1723	0.8	-7.53	55.4	1.66	17.51	2.45	0.01	9.34	9.99	2.36	0.53	0.00	0.0	1240	Ir14	13	anhydrous
1723	0.8	-7.53	54.0	1.63	17.63	4.72	0.01	9.38	10.01	2.29	0.48	0.00	0.0	1180	Ir15	13	anhydrous
1723	0.8	-7.53	55.5	1.70	17.55	2.50	0.01	9.36	9.96	2.41	0.58	0.00	0.0	1160	Pd7	13	anhydrous
1723	0.8	-7.53	54.5	1.64	17.36	4.61	0.01	9.19	9.76	2.20	0.52	0.00	0.0	1080	Ir16	13	anhydrous
1723	0.8	-7.53	54.5	1.66	17.43	4.55	0.00	9.12	9.79	2.22	0.54	0.00	0.0	970	Pd9	13	anhydrous
1473	0.0001	-11.96	36.6	0.58	13.29	32.78	0.21	6.06	7.28	0.82	0.10	0.54	0.0	6420	SS9	14	anhydrous
1573	0.8	-7.45	45.3	1.44	8.10	27.77	0.36	3.10	8.36	2.34	0.46	1.11	0.0	5540	20	14	anhydrous
1723	0.8	-6.17	52.4	0.76	4.60	17.17	0.20	10.20	10.76	1.48	0.30	0.63	0.0	5230	6	14	anhydrous
1523	0.0001	-11.34	38.8	0.85	17.70	29.80	0.20	3.20	6.70	1.20	0.14	0.28	0.0	5000	SS3	14	anhydrous
1573	0.0001	-10.77	37.7	0.65	18.70	26.40	0.23	6.10	7.23	0.88	0.14	0.49	0.0	4500	SS7	14	anhydrous
1673	0.8	-6.57	51.1	0.61	4.60	15.09	0.21	12.40	11.84	1.11	0.13	0.61	0.0	3330	13	14	anhydrous
1623	0.8	-7.00	53.0	0.78	5.80	13.99	0.22	11.80	11.00	1.16	0.19	0.63	0.0	3210	16	14	anhydrous
1573	0.8	-7.45	49.5	0.66	7.60	18.07	0.34	9.20	11.78	1.18	0.20	0.64	0.0	3170	21	14	anhydrous
1773	0.8	-6.19	54.1	1.20	4.96	9.30	0.15	20.33	7.44	1.82	0.32	0.74	0.0	2970	5-6	14	anhydrous

1773	0.8	-5.79	54.9	1.78	6.02	17.23	0.17	6.31	9.08	1.63	0.41	0.77	0.0	2830	29	14	anhydrous
1673	0.8	-6.97	51.8	0.60	5.00	5.74	0.14	18.90	14.01	1.18	0.18	0.70	0.0	2630	7	14	anhydrous
1723	0.8	-6.57	49.4	0.96	7.40	8.23	0.00	17.70	13.12	0.89	0.17	0.64	0.0	2430	4	14	anhydrous
1623	0.8	-7.40	50.2	0.77	7.80	4.27	0.10	16.50	15.26	1.44	0.27	1.17	0.0	2250	8	14	anhydrous
1773	0.8	-6.19	53.9	1.05	5.01	10.92	0.17	22.39	5.96	0.97	0.23	0.78	0.0	2220	5-3	14	anhydrous
1523	0.0001	-11.34	44.4	0.81	19.20	15.37	0.24	8.10	8.84	1.14	0.24	0.65	0.0	2010	SS6	14	anhydrous
1603	1	-9.50	52.1	1.80	14.55	10.09	0.18	8.12	9.18	2.75	0.00	0.00	0.0	1430	PGE1b	15	anhydrous
1603	1	-9.20	50.7	1.78	14.07	10.75	0.16	7.59	9.05	3.78	0.00	0.00	0.0	1320	PGE1d	15	anhydrous
1603	1	-9.20	51.9	1.92	14.25	9.82	0.18	8.04	9.38	2.57	0.00	0.00	0.0	1220	PGE1c	15	anhydrous
1603	1	-8.90	52.3	1.73	15.21	10.17	0.19	7.97	9.11	2.75	0.00	0.00	0.0	930	IPRe4	15	anhydrous

Sources:

1: This study, 2. Baker et al. (2001), 3. Beermann et al. (2011), 4. Brenan (2008), 5. Ding et al. (2014), 6. Haughton et al. (1974), 7. Holzhiel & Grove (2002), 8. Jugo et al. (2005), 9. Liu et al. (2007), 10. Mavrogenes & O'Neill (1999), 11. Moune et al. (2009), 12. Peach & Mathez (1993), 13. Peach et al. (1994), 14. Richter et al. (2009), 15. Sattari et al. (2002)

APPENDIX II: Test Dataset

T(K)	P (GPa)	log fO ₂	SiO ₂	TiO ₂	Al ₂ O ₃	FeO*	MnO	MgO	CaO	Na ₂ O	K ₂ O	H ₂ O		S ppm	run#	Source	water method
												P ₂ O ₅	wt. %				
1473	0.0001	-9.04	55.5	1.85	15.05	7.39	0.11	8.89	9.28	2.39	0.00	0.00	0.0	957	fO2#3e	1	anhydrous
1473	0.0001	-12.04	57.0	2.63	20.47	1.78	0.00	7.25	7.07	2.99	1.44	0.00	0.0	420	12F2	2	anhydrous
1473	0.0001	-9.40	45.7	1.83	20.08	15.44	0.00	5.64	7.99	2.69	1.30	0.00	0.0	1360	6F1	2	anhydrous
1623	1	-11.19	44.7	0.00	16.20	11.90	0.00	8.08	16.80	0.00	0.00	0.00	0.0	1690	FES-BK11	3	anhydrous
1628	1.6	-7.39	47.1	0.68	17.80	8.20	0.00	12.60	10.70	2.10	0.00	0.00	0.0	1800	10	4	anhydrous
1573	1	-8.45	77.9	0.11	13.01	0.71	0.09	0.08	0.59	3.81	4.61	0.00	0.0	182	TS8	5	anhydrous
1623	1	-8.06	76.3	0.11	13.20	0.76	0.00	0.07	0.56	5.31	4.72	0.00	0.0	186	TS12	5	anhydrous
1523	1	-8.87	64.1	0.61	16.43	5.19	0.00	2.00	4.78	4.45	1.98	0.00	0.0	482	TS5	5	anhydrous
2073	5.5	-5.10	50.2	1.60	17.21	10.22	0.00	7.40	10.11	1.90	0.90	0.00	0.0	1335	MAV69	6	anhydrous
1723	0.8	-7.53	57.0	1.40	18.38	1.95	0.00	8.70	9.79	2.09	0.49	0.00	0.0	1309	Ni17	7	anhydrous
1723	0.8	-7.53	50.9	1.51	16.98	8.94	0.01	8.63	9.39	2.23	0.51	0.00	0.0	1800	Pd12	8	anhydrous
1673	0.8	-6.97	66.9	1.60	6.12	4.78	0.04	7.22	7.12	3.83	1.06	1.03	0.0	981	5-4	9	anhydrous
1603	1	-9.3	51.5	1.77	14.41	9.50	0.15	7.82	9.16	2.85	0.00	0.00	0.0	1240	PGE1e	10	anhydrous
1323	0.299	-10.07	46.6	3.55	14.74	12.97	0.24	4.26	8.83	3.16	0.65	0.64	2.6	1210	B-16	11	corrected KFT

Sources:

1. Brenan (2008), 2. Haughton et al. (1974), 3. Holzheid & Grove (2002), 4. Jugo et al. (2005), 5. Liu et al. (2007), 6. Mavrogenes & O'Neill (1999), 7. Peach & Mathez (1993), 8. Peach et al. (1994), 9. Richter et al. (2009), 10. Sattari et al. (2002), 11. Moune et al. (2009)

APPENDIX III: Indirect Water Measurements Dataset

T(K)	P (GPa)	log fO ₂	SiO ₂	TiO ₂	Al ₂ O ₃	FeO*	MnO	MgO	CaO	Na ₂ O	K ₂ O	H ₂ O		S ppm	run#	Source	water method
												P ₂ O ₅	wt. %				
1473	0.2	-8.2	45.8	1.53	14.47	9.77	0.14	10.49	9.32	2.94	1.62	0.48	3.5	3000	S18	1	By difference EMPA
1423	0.2	-8.4	46.0	1.61	15.05	10.38	0.13	8.47	9.81	3.09	1.80	0.49	3.2	3100	S19	1	By difference EMPA
1423	0.2	-8.6	46.2	1.64	15.26	10.19	0.24	8.24	9.87	3.07	1.80	0.52	3.1	2700	S20	1	By difference EMPA
1423	0.2	-7.6	45.4	1.41	13.19	10.71	0.21	13.47	8.41	2.58	1.48	0.46	2.8	3900	S21	1	By difference EMPA
1058	0.2152	-17.39	77.5	0.00	13.71	0.17	0.00	0.32	1.98	4.34	1.94	0.00	5.9	126	MP15X	2	By difference EMPA
1058	0.2152	-17.54	78.0	0.00	13.51	0.23	0.00	0.34	1.77	4.27	1.92	0.00	4.6	96	MP15SN	2	By difference EMPA
1071	0.1973	-14.79	78.8	0.00	12.31	0.16	0.00	0.33	1.45	2.87	4.10	0.00	5.0	108	MP16I	2	By difference EMPA
1084	0.1976	-13.99	80.0	0.00	12.06	0.10	0.00	0.37	1.41	3.89	2.15	0.00	5.9	125	MP17I	2	By difference EMPA
1084	0.1976	-13.99	77.8	0.00	13.42	0.40	0.00	0.31	1.99	4.19	1.95	0.00	6.2	83	MP17VII7	2	By difference EMPA
1203	0.2054	-12.19	76.9	0.00	13.62	0.48	0.00	0.35	2.07	4.57	1.99	0.00	5.0	158	MP2I	2	By difference EMPA
1203	0.2054	-12.29	75.8	0.00	13.34	2.41	0.00	0.33	1.95	4.22	1.92	0.00	4.4	112	MP2II	2	By difference EMPA
1203	0.2054	-12.24	77.3	0.00	13.55	0.45	0.00	0.35	2.01	4.43	1.94	0.00	4.7	285	MP2III	2	By difference EMPA
1206	0.2257	-11.10	77.3	0.00	13.73	1.85	0.00	0.32	0.39	4.40	2.01	0.00	3.0	989	MP3I	2	By difference EMPA
1206	0.2257	-11.22	76.9	0.00	13.50	1.81	0.00	0.33	1.18	4.37	1.90	0.00	2.8	307	MP3II	2	By difference EMPA
1206	0.2257	-10.61	76.2	0.00	13.40	1.93	0.00	0.33	2.10	4.05	1.96	0.00	4.9	186	MP3III	2	By difference EMPA
1205	0.1986	-15.13	77.2	0.00	13.66	0.19	0.00	0.32	2.04	4.60	1.99	0.00	3.7	313	MP4I	2	By difference EMPA
1205	0.1986	-14.93	75.6	0.00	13.38	0.43	0.00	0.20	4.23	4.28	1.93	0.00	4.4	148	MP4III	2	By difference EMPA
1209	0.2116	-11.32	76.9	0.00	13.54	1.16	0.00	0.32	2.02	3.99	2.12	0.00	4.7	77	MP9I	2	By difference EMPA
1206	0.2013	-14.91	77.3	0.00	13.52	0.31	0.00	0.30	2.04	4.38	2.10	0.00	4.5	189	MP10I	2	By difference EMPA
1208	0.2202	-14.14	77.3	0.00	13.40	0.34	0.00	0.32	2.04	4.48	2.11	0.00	4.4	211	MP11I	2	By difference EMPA
1207	0.2003	-13.85	76.8	0.00	13.67	1.06	0.00	0.35	1.97	3.99	2.16	0.00	4.5	72	MP6II	2	By difference EMPA
1207	0.2003	-13.97	77.3	0.00	13.77	0.44	0.00	0.35	2.00	4.02	2.08	0.00	4.1	74	MP6III	2	By difference EMPA
1203	0.2001	-12.11	77.3	0.00	13.94	0.38	0.00	0.31	1.79	4.39	1.88	0.00	2.5	371	MP13I	2	By difference EMPA
1203	0.2001	-12.16	77.2	0.00	13.97	0.31	0.00	0.30	1.72	4.63	1.86	0.00	2.5	422	MP13II	2	By difference EMPA
1203	0.2001	-12.58	77.2	0.00	13.87	0.29	0.00	0.38	1.89	4.53	1.85	0.00	1.8	429	MP13IV	2	By difference EMPA

1267	0.2188	-13.83	77.3	0.00	13.73	0.46	0.00	0.34	2.02	4.23	1.89	0.00	3.4	284	MP18I	2	By difference EMPA
1267	0.2188	-13.48	77.1	0.00	13.68	0.92	0.00	0.32	2.07	4.12	1.80	0.00	4.2	147	MP18II	2	By difference EMPA
1267	0.2188	-13.89	77.5	0.00	13.69	0.26	0.00	0.33	2.07	4.26	1.87	0.00	3.8	453	MP18IV	2	By difference EMPA
1267	0.2188	-13.30	76.7	0.00	13.67	1.09	0.00	0.33	2.07	4.24	1.90	0.00	4.8	178	MP18XII	2	By difference EMPA
1267	0.2188	-13.29	76.3	0.00	13.72	1.50	0.00	0.32	2.03	4.20	1.90	0.00	4.5	116	MP18SN6	2	By difference EMPA
1269	0.2068	-11.27	76.4	0.00	13.54	1.46	0.00	0.35	2.08	4.28	1.91	0.00	3.6	132	MP19III	2	By difference EMPA
1269	0.2068	-10.93	76.3	0.00	13.47	2.09	0.00	0.35	2.14	3.74	1.92	0.00	5.2	122	MP19X	2	By difference EMPA
1269	0.2068	-10.93	76.4	0.00	13.57	1.84	0.00	0.33	2.06	3.90	1.89	0.00	4.7	145	MP19XI	2	By difference EMPA
1269	0.2068	-10.99	75.4	0.00	13.44	3.06	0.00	0.32	2.03	3.85	1.93	0.00	4.4	167	MP19XII	2	By difference EMPA
1260	0.1992	-10.43	76.7	0.00	13.67	2.20	0.00	0.34	1.30	3.93	1.84	0.00	2.8	674	MP14I	2	By difference EMPA
1260	0.1992	-10.48	76.9	0.00	13.73	2.13	0.00	0.32	1.24	3.90	1.79	0.00	2.7	563	MP14II	2	By difference EMPA
1260	0.1992	-10.81	77.6	0.00	13.90	0.92	0.00	0.35	1.15	4.16	1.92	0.00	2.1	734	MP14III	2	By difference EMPA
1260	0.1992	-10.66	77.6	0.00	14.02	0.63	0.00	0.33	1.18	4.34	1.89	0.00	1.8	771	MP14IV	2	By difference EMPA
1260	0.1992	-10.63	75.9	0.00	13.35	3.17	0.00	0.30	1.62	3.88	1.79	0.00	2.5	399	MP14VI6	2	By difference EMPA
1260	0.1992	-10.30	76.1	0.00	13.48	3.26	0.00	0.31	1.15	3.90	1.81	0.00	3.2	645	MP14VII	2	By difference EMPA
1260	0.1992	-10.52	78.7	0.00	12.99	0.89	0.00	0.23	1.19	3.28	2.76	0.00	2.6	186	PIN14VIII	2	By difference EMPA
1206	0.2013	-14.98	77.4	0.00	13.60	0.13	0.00	0.32	1.99	1.39	2.15	0.00	4.3	544	MP10II	2	By difference EMPA
1058	0.2152	-18.29	78.6	0.00	12.57	0.18	0.00	0.18	0.67	3.92	3.88	0.00	2.6	753	MP15IV	2	By difference EMPA
1267	0.2188	-14.30	77.2	0.00	13.80	0.16	0.00	0.31	2.10	4.53	1.88	0.00	2.6	660	MP18V	2	By difference EMPA
1071	0.1973	-15.11	77.3	0.00	12.50	0.10	0.00	0.34	0.65	3.02	6.16	0.00	3.7	356	MP16IV	2	By difference EMPA
1206	0.2013	-15.01	77.7	0.00	13.35	0.20	0.00	0.32	1.95	4.38	2.08	0.00	4.1	691	MP10III	2	By difference EMPA
1084	0.1976	-13.99	79.9	0.00	12.13	0.08	0.00	0.40	1.21	3.93	2.32	0.00	5.9	263	MP17II	2	By difference EMPA
1058	0.2152	-17.52	78.5	0.00	13.08	0.14	0.00	0.27	1.01	4.44	2.52	0.00	4.7	440	MP15II	2	By difference EMPA
1207	0.2092	-13.11	77.4	0.00	13.53	0.09	0.00	0.34	2.01	4.45	2.13	0.00	4.4	273	MP12I	2	By difference EMPA
1207	0.2092	-13.10	77.3	0.00	13.62	0.12	0.00	0.33	2.05	4.39	2.15	0.00	4.5	334	MP12II	2	By difference EMPA
1084	0.1976	-13.99	79.9	0.00	12.17	0.11	0.00	0.40	1.12	3.98	2.32	0.00	5.5	304	MP17III	2	By difference EMPA
1071	0.1973	-15.02	78.1	0.00	12.28	0.10	0.00	0.37	0.85	2.98	5.39	0.00	4.0	274	MP16V	2	By difference EMPA
1267	0.2188	-14.81	77.0	0.00	13.51	0.27	0.00	0.33	2.09	4.89	1.90	0.00	1.8	698	PIN18IX	2	By difference EMPA
1084	0.1976	-14.03	79.1	0.00	13.04	0.11	0.00	0.22	1.05	3.30	3.22	0.00	5.4	281	PIN17VI	2	By difference EMPA

1071	0.1973	-14.93	78.1	0.00	12.16	0.10	0.00	0.36	0.99	3.02	5.27	0.00	4.3	240	MP16III	2	By difference EMPA
1203	0.2001	-12.35	77.8	0.00	13.75	0.21	0.00	0.33	1.70	4.38	1.87	0.00	2.1	494	MP13III	2	By difference EMPA
1084	0.1976	-14.02	79.9	0.00	12.23	0.12	0.00	0.40	1.06	3.94	2.33	0.00	5.5	279	MP17IV	2	By difference EMPA
1123	2	-13.16	71.3	0.20	14.58	0.95	0.00	0.31	0.85	0.98	1.50	0.00	9.4	69	G195	3	By difference EMPA
1173	2	-12.04	67.3	0.11	14.30	1.04	0.00	0.27	1.22	1.23	2.24	0.00	12.3	155	G190	3	By difference EMPA
1198	2	-11.66	67.1	0.28	13.84	1.39	0.00	0.33	1.01	2.13	2.69	0.00	11.2	146	G207	3	By difference EMPA
1223	2	-11.44	69.0	0.30	14.77	1.29	0.00	0.30	0.93	1.75	2.64	0.00	9.0	69	G193	3	By difference EMPA
1283	2	-10.57	67.4	0.55	14.25	2.00	0.00	0.49	1.31	4.27	1.57	0.00	8.2	119	B93	3	By difference EMPA
1323	2	-9.89	64.6	0.71	14.64	2.64	0.00	0.72	1.67	4.08	1.40	0.00	9.5	155	B85	3	By difference EMPA
1223	3	-11.62	72.7	0.34	13.73	1.09	0.00	0.28	0.81	0.96	3.00	0.00	7.1	62	G223	3	By difference EMPA
1323	3	-9.8	67.9	0.79	11.72	2.18	0.00	0.41	1.29	1.57	3.91	0.00	10.2	60	G224	3	By difference EMPA
1173	2	-13.98	68.2	0.26	13.60	1.27	0.00	0.34	0.91	2.43	1.80	0.00	11.1	103	G218	3	By difference EMPA
1223	2	-13.13	65.0	0.41	13.90	1.85	0.00	0.41	1.12	4.76	1.50	0.00	11.1	108	G203	3	By difference EMPA
1273	2	-12.68	67.9	0.46	14.29	1.72	0.00	0.34	0.85	4.48	2.68	0.00	7.3	90	B87	3	By difference EMPA
1323	2	-12.16	66.4	0.74	15.09	2.32	0.00	0.50	1.17	6.23	1.85	0.00	5.7	97	G202	3	By difference EMPA
1173	3	-14.41	71.2	0.32	13.02	1.13	0.00	0.51	1.15	0.87	3.58	0.00	8.2	78	G225	3	By difference EMPA
1248	3	-13	68.9	0.61	12.29	1.68	0.00	0.39	1.11	0.95	4.14	0.00	9.9	136	G228	3	By difference EMPA
1323	3	-11.82	68.5	0.82	11.96	2.49	0.00	0.37	0.96	1.28	2.95	0.00	10.7	111	G230	3	By difference EMPA
1523	1	-8.87	47.3	1.64	16.66	9.75	0.16	6.01	10.43	3.29	1.84	0.55	2.8	1231	yn87	4	Added water
1523	1	-8.87	58.9	0.79	15.92	7.71	0.22	1.96	5.57	3.95	1.96	0.39	3.5	723	yn88	4	Added water
1523	1	-8.87	72.9	0.10	12.42	1.02	0.08	0.07	0.54	4.19	4.54	0.01	2.9	326	yn89	4	Added water
1523	1	-8.87	73.6	0.10	12.51	0.78	0.08	0.07	0.54	4.19	4.55	0.01	6.1	373	yn90	4	Added water
1423	1	-9.79	58.5	0.82	15.86	9.02	0.26	2.14	5.80	4.13	1.87	0.37	2.9	506	yn91	4	Added water
1423	1	-9.79	59.4	0.92	14.39	9.50	0.25	2.23	5.14	3.76	2.24	0.43	2.8	534	yn93	4	Added water
1523	1	-8.87	48.0	1.71	16.85	8.96	0.18	6.00	10.59	3.30	1.85	0.55	4.0	663	Yn108	4	Added water
1523	1	-8.87	62.8	0.52	17.49	4.83	0.01	1.71	5.32	4.13	1.74	0.02	6.4	419	Yn109	4	Added water
1523	1	-8.87	63.8	0.54	17.76	4.68	0.01	1.63	5.22	4.29	1.82	0.01	8.5	316	Yn110	4	Added water
1323	1	-8.13	70.8	0.11	12.14	1.45	0.07	0.07	0.53	4.19	3.73	0.01	8.8	700	yn104	4	Added water
1223	0.2	-10.93	57.4	0.63	18.96	6.06	0.21	1.93	6.86	4.75	3.03	0.00	6.1	561	198	5	albite-H2O Burnham

1273	0.2	-10.16	58.0	0.66	18.89	6.09	0.21	1.45	8.32	4.15	2.17	0.00	6.0	400	161	5	albite-H2O Burnham
1173	0.4	-11.60	59.3	0.52	19.72	5.08	0.19	1.05	6.30	4.48	3.29	0.00	8.2	280	223	5	albite-H2O Burnham
1173	0.2	-11.76	59.7	0.48	19.37	5.53	0.18	0.99	5.35	4.86	3.44	0.00	6.1	440	185	5	albite-H2O Burnham
1273	0.2	-10.16	60.3	0.45	22.41	2.96	0.09	0.34	6.80	5.38	1.22	0.00	6.1	440	163	5	albite-H2O Burnham
1273	0.4	-10.02	61.3	0.44	22.20	1.96	0.12	0.36	7.45	5.09	0.99	0.00	8.1	120	260	5	albite-H2O Burnham
1223	0.2	-10.93	63.6	0.62	21.38	1.93	0.10	0.28	4.97	5.50	1.57	0.00	6.1	280	200	5	albite-H2O Burnham
1173	0.1	-11.84	64.4	0.29	17.27	4.30	0.21	0.62	2.28	5.51	5.12	0.00	4.2	160	286	5	albite-H2O Burnham
1223	0.4	-10.78	64.6	0.20	21.55	1.54	0.12	0.37	6.11	4.20	1.23	0.00	8.1	80	275	5	albite-H2O Burnham
1123	0.2	-12.66	65.0	0.01	17.98	3.78	0.02	0.40	2.48	5.43	4.85	0.00	6.1	360	148	5	albite-H2O Burnham
1123	0.2	-12.66	65.2	0.29	17.60	3.57	0.18	0.42	2.88	5.06	4.74	0.00	6.0	240	144	5	albite-H2O Burnham
1073	0.4	-13.48	66.1	0.21	18.35	1.92	0.17	0.29	3.25	4.90	4.78	0.00	8.3	80	218	5	albite-H2O Burnham
1173	0.2	-11.76	67.1	0.24	18.71	2.33	0.09	0.39	3.47	5.50	2.05	0.00	6.0	320	187	5	albite-H2O Burnham
1123	0.4	-12.50	67.4	0.12	19.00	2.14	0.08	0.64	4.00	5.04	1.56	0.00	8.1	120	230	5	albite-H2O Burnham
1073	0.2	-13.65	68.3	0.02	16.78	2.17	0.02	0.18	1.46	5.23	5.76	0.00	6.1	200	156	5	albite-H2O Burnham
1123	0.2	-12.66	69.4	0.13	17.36	1.69	0.05	0.57	2.17	5.45	3.08	0.00	6.0	280	146	5	albite-H2O Burnham
1073	0.4	-13.48	70.1	0.10	17.30	1.79	0.09	0.65	2.99	4.99	1.98	0.00	8.0	120	220	5	albite-H2O Burnham
1173	0.4	-11.60	65.3	0.11	20.81	2.18	0.09	0.60	4.93	4.64	1.33	0.00	8.2	120	225	5	albite-H2O Burnham
1073	0.2	-13.65	69.3	0.21	16.16	1.94	0.12	0.16	1.70	4.84	5.51	0.00	6.0	200	153	5	albite-H2O Burnham
1123	0.4	-12.50	62.4	0.30	19.65	3.20	0.18	0.47	5.25	4.85	3.67	0.00	8.2	80	228	5	albite-H2O Burnham
1073	0.2	-13.65	72.2	0.12	15.50	1.34	0.03	0.45	1.45	5.53	3.33	0.00	6.0	240	155	5	albite-H2O Burnham
1073	0.2	-14.585	72.2	0.09	11.40	0.32	0.01	0.02	0.69	3.02	4.62	0.00	7.3	148	196	6	albite-H2O Burnham
1173	0.2	-12.6121	72.8	0.07	11.63	0.51	0.02	0.02	0.67	3.03	4.75	0.00	6.5	126	197	6	By difference EMPA
1273	0.2	-10.9491	65.2	0.48	14.53	2.46	0.02	1.00	1.75	2.50	5.41	0.00	6.5	145	199	6	By difference EMPA
1273	0.2	-10.9491	55.9	0.61	17.31	5.92	0.19	2.86	6.48	3.27	0.79	0.00	6.6	354	200	6	By difference EMPA
1273	0.2	-10.9491	52.1	1.12	14.95	9.87	0.21	3.97	9.24	2.09	0.42	0.00	5.9	670	201	6	By difference EMPA

Sources:

1. Beermann et al. (2011), 2. Clemente et al. (2004), 3. Jago & Dasgupta (2013), 4. Liu et al. (2007), 5. Luhr (1990), 6. Zajacz et al. (2013)